Isotope dependence of energy, momentum and particle confinement in tokamaks

H. Weisen[1], C.F. Maggi[2], M. Oberparleiter[3], F.J. Casson[2], Y. Camenen[4], S. Menmuir[2], L Horvath[2,5], F. Auriemma[6], T.W. Bache[2], N. Bonanomi[7], A. Chankin[7], E. Delabie[8], Frassinetti[9], J. Garcia[10], C. Giroud[2], D. King[2], R Lorenzini[6], M. Marin[11], P.A. Schneider[7], P. Siren[12,13], J. Varje[13], E. Viezzer[14] and JET contributors*

[1]Ecole Polytechnique Fédérale de Lausanne (EPFL), Swiss Plasma Center (SPC), CH-1015 Lausanne, Switzerland
[2]CCFE, Culham Science Centre, Abingdon OX14 3DB, UK,
[3]Chalmers University of Technology, SE-412 96 Gothenburg, Sweden
[4]CNRS, Aix-Marseille Univ., PIIM UMR7345, Marseille, France
[5]York Plasma Institute, Department of Physics, University of York, York YO10 5DD, UK,
[6]Consorzio RFX, Corso Stati Uniti 4, I-35127 Padova, Italy,
[7]Max-Planck Institut für Plasmaphysik, D-85748 Garching, Germany,
[8]Oak Ridge National Laboratory, Tennessee USA,
[9]Royal Institute of Technology KTH, SE-10044 Stockholm, Sweden
[10]CEA, Cadarache, France,
[11]DIFFER, Dutch Institute for Fundamental Energy Research, Eindhoven, Netherlands
[12]Aalto University, Espoo, Finland,
[11]DIFFER - Dutch Institute for Fundamental Energy Research, Eindhoven, the Netherlands
[13]VTT, Espoo, Finland,
[14]University of Sevilla, Spain
*See the author list of E. Joffrin et al., 2019 Nucl. Fusion 59 112021

Abstract

The isotope dependence of plasma transport will have a significant impact on the performance of future D-T experiments in JET and ITER and eventually on the fusion gain and economics of future reactors. In preparation for future D-T operation on JET, dedicated experiments and comprehensive transport analysis were performed in H, D and H-D mixed plasmas. The analyses of the data has demonstrated an unexpectedly strong and favourable dependence of the global confinement of energy, momentum and particles in ELMy H-mode plasmas on the atomic mass of the main ion species, scaling as $\tau_E \sim A^{0.5}$ [C.F. Maggi 2018, JET Team 1999], i.e. opposite to the expectations based only on local gyro-Bohm (GB) scaling, $\tau_E \sim A^{-0.5}$, and stronger than in the commonly used H-mode scaling for the energy confinement [G. Saibene 1999, ITER Physics Basis 1999]. The scaling of momentum transport and particle confinement with isotope mass is very similar to that of energy transport. Nonlinear local GENE gyrokinetic analysis shows that the observed anti-GB heat flux is accounted for if collisions, $E \times B$ shear and plasma dilution with low-Z impurities (^9Be) are included in the analysis.
For L-mode plasmas a weaker positive isotope scaling $\tau_E \sim A^{0.14}$ has been found in JET [C.F. Maggi 2018], similar to ITER97-L scaling [S. M. Kaye 1997]. Flux-driven quasi-linear gyrofluid calculations using JETTO-TGLF in L-mode show that local GB scaling is not followed when stiff transport (as is the case for ITGs) is combined with an imposed boundary condition taken from the experiment, in this case predicting no isotope dependence. A dimensionless identity plasma pair in hydrogen and deuterium L-mode plasmas has demonstrated scale invariance, confirming that core transport physics is governed, as expected, by 4 dimensionless parameters (ρ^*, ν^*, β, q), consistently with global quasi-linear gyrokinetic TGLF calculations [Maggi 2019].
We compare findings in JET with those in different devices and discuss the possible reasons for the different isotope scalings reported from different devices. The diversity of observations suggests that the differences may result not only from differences affecting the core, e.g. heating schemes, but are to a large part due to differences in device-specific edge and wall conditions, pointing to the importance of better understanding and controlling pedestal and edge processes.

1) Introduction

While most current devices use deuterium as an operating main plasma species, an eventual reactor will use deuterium-tritium mixtures. This has motivated several experimental studies (many historic) on the effects of the main species isotope on plasma properties, albeit restricted to comparisons between deuterium and hydrogen, except for JET-C [Bessenrodt 1993, C.F. Maggi 2018, JET Team, 1999, G. Saibene 1999, J.G. Cordey1999, H. Weisen 2018, C.F. Maggi 2019], and TFTR [Scott 1995, Ernst 1998]. We will refer to JET as JET-C for the period when JET was operated with carbon plasma facing components, i.e up to 2009 and as JET-ILW beyond 2010, when JET was equipped with a tungsten divertor and Be main chamber limiters [Matthews 2011].

In early experiments in ASDEX and in several other devices, thoroughly reviewed in ref [Bessenrodt], very significant positive dependencies on the isotope mass were observed. Deuterium plasmas in ASDEX had significantly better confinement than hydrogen plasmas in all confinement regimes and heating modes. Indeed, some improved confinement regimes were inaccessible with hydrogen operation [Bessenrodt]. Deuterium H-modes in ASDEX were reported to have a confinement time twice that of H-modes in hydrogen, while in L-mode the improvement was weaker, but still substantial (a factor 1.4). TFTR reported a strong L-mode scaling of the thermal confinement time $\tau_E = W_{tot}/P_{loss} \propto A^{0.5}$ [Scott 1995], and a very strong scaling in the supershot regime $\tau_E \propto A^{0.85}$ [Ernst 1998], based on a comparison of deuterium and deuterium-tritium mixtures. A is the atomic mass number, $W_{tot}=1.5\int(n_eT_e+n_iT_i)dV$, the thermal stored energy, P_{loss} is the power transported through the last closed flux surface (LCFS). T_e and T_i are the electron and ion temperatures, n_e and n_i being their densities.

The popular IPB98(y,2) ELMy H-mode thermal energy scaling [ITER Physics Basis 1999 & 2007], the underlying dataset of which includes data from tritium and deuterium-tritium mixtures from the JET-C DTE1 campaign [G. Saibene 1999] in 1997 exhibit however only a weak scaling, $\tau_E \propto A^{0.19}$. This is close to the one for L-mode, $\tau_E \propto A^{0.2}$ [ITER Physics Basis 1999]. The weak ELMy H-mode scaling contrasts with a relatively strong scaling of the ELM-free confinement time reported in [ITER Physics Basis 1999], $\tau_E \propto A^{0.43}$, hinting at the role of the H-mode edge pedestal. While global scaling from international databases [ITER Physics Basis 1999 & 2007, G. Verdolaege 2018] use very diverse datasets, which are susceptible to correlations between scaling variables, experiments with matched or at least similar sets of data with different species can provide different results. This was the case of the global confinement time of a small set of JET-C pulses of similar density in H, D and T, for which no significant isotope dependence was found: $\tau_E \propto A^{0.03}$ [J.G. Cordey 1999]. Two term scalings, separating core and pedestal thermal confinement in H-mode, have been reported to have a very strong pedestal scaling $\tau_{E,ped} \propto A^{0.96}$ and a weak negative dependence of the plasma core confinement $\tau_{E,core} \propto A^{-0.16}$ [J.G. Cordey 1999]. Here $\tau_{E,ped} = W_{ped}/P_{loss}$, with $W_{ped}=1.5(n_{eped}T_{eped}+n_{iped}T_{iped})V_{top}$ where subscript *ped* refers to the values at the pedestal top, which is typically 1-3cm inward from the LCFS in JET [Maggi 2017], $V_{top} \approx V$ is the volume inside the flux surface defined by the pedestal top and V the total plasma volume. The core confinement time is defined as $\tau_{E,core} = \tau_E - \tau_{E,ped}$. The scalings reported by ref [J.G. Cordey 1999] are at odds with more recent experimental results [Maggi 2018] and the now well documented and understood transport property of profile stiffness [Garbet 2004, Citrin 2014]. Profile stiffness, leads to a proportionality of the total thermal stored energy content and the pedestal thermal energy content, i.e. $W_{tot} = \propto W_{ped}$. Here n_e and n_i are the local electron and ion densities, T_e and T_i their temperatures; the integral extends over the plasma volume and P_{loss} is the power transported by the plasma through the separatrix. (In the above expression we have neglected the fact that the pedestal top is typically 1-3cm inward from the separatrix). Core ion profile stiffness can however be broken, generally with high neutral beam heating (NBH) power, by core transport processes such as E×B shear stabilisation [H. Biglari 1999, M.N. Rosenbluth 1998, T.S. Hahm 1995, T.S. Hahm 1996, R.E. Waltz 1998] and fast ion stabilisation [J. Citrin 2014, J. Citrin 2015, J. Garcia 2015, Di Siena 2018] of ITG's, leading to a core confinement improvement beyond that expected from the pedestal alone. The

international ITPA confinement databases have recently been revised and now include new data in hydrogen from ASDEX-upgrade and JET-ILW [G. Verdoolaege 2018]. Exponents for the isotope mass range from 0.09 to 0.47, depending on the datasets and regression methods used.

After the TFTR and JET-C D-T campaigns, isotope effects received little attention for an entire decade until experiments in JT-60U with high quality diagnostics showed a clear dependence of the ion heat flux on the main isotope in H-mode, hydrogen plasmas requiring about twice as much power as deuterium plasmas in order to achieve the same stored energy [H. Urano 2012 & 2013].

Overall, these results have painted a rather confusing picture of the dependence of the energy confinement time on the isotope mass. The bewildering range of results reported suggests that what is commonly referred to as 'isotope effects' may result from a number of effects linked to the usage of different working gases as much as from intrinsic transport physics. However, what virtually all observations have in common, is an improvement of global energy confinement with ion mass, in apparent contradiction with simple theoretical estimates, which predict gyroBohm scaling, i.e. $\tau_E \propto A^{-1/2}$ [Perkins 1993]. Some of the incongruities of early results may be linked diagnostics limitations, such as the lack of spatial resolution for resolving the H-mode pedestal. Diagnostic quality and the resolution for pedestal measurements has greatly improved since, as has our understanding of transport, prompting a revisit of the 'isotope effect' during the last decade in several devices.

2) Effects depending on working gas isotope

2.1 Transport physics effects

There are numerous basic plasma parameters that depend on the ion mass number. These include the thermal velocity $v_i = (T_i/m_i)^{1/2}$ where $m_i = A m_p$, m_p being the proton mass, the ion Larmor radius $\rho_i = v_i/\omega_{ci}$, $\omega_{ci} = ZeB/(A m_p)$ being the ion cyclotron frequency, the Alfvén velocity $v_A = B/(\mu_0 n_i m_i)^{1/2}$, the ion-ion collision frequency v_{ii} and electron-ion momentum and energy exchange frequencies v_{ei} and v^E_{ei} (for a single ion species plasma)

$$v_{ii} = \frac{n_i Z^4 e^4 \ln\Lambda}{8\sqrt{2}\pi\epsilon_0^2 m_i^2 v_i^3} \propto A^{-1/2} \qquad v_{ei} = \frac{n_i Z^2 e^4 \ln\Lambda}{8\sqrt{2}\pi\epsilon_0^2 m_e^2 v_e^3} \propto A^0 \qquad v^E_{ei} = \frac{2 m_e}{m_i} v_{ei} \propto A^{-1}$$

as well as the electron-ion heat exchange power density $q_{ei} = 1.5 n_e v^E_{ei}(T_e - T_i) \propto A^{-1}$. In the above B is the magnetic field, n_i is the ion density, Z the atomic charge number, n_e the electron density, $v_e = (T_e/m_e)^{1/2}$ the electron thermal velocity and $\ln\Lambda$ is the Coulomb logarithm [Huba 2013].

We loosely follow ref. [Horton 1999] to introduce the basic expectation for the scaling of the cross-field diffusion coefficient D and heat diffusivity χ for drift wave turbulence $D \sim \chi \sim \Delta_r^2/\delta t$, where Δ_r is the characteristic turbulent radial scale length and $\delta_t \approx L_\theta/v_d \approx L_\theta/(T/eZBL_r)$ its characteristic time scale, $v_d = T/(eZBL_r)$ the drift velocity with L_r a radial profile gradient length such as $L_n = -n/\nabla_r n$ or $L_T = -T/\nabla_r T$. L_θ is the poloidal scale length related to the poloidal mode number m as

$L_\theta \approx 2\pi a/m$, whre a is the plasma minor radius. This leads to $\chi \sim \dfrac{T}{eZB} \dfrac{\Delta_r^2}{L_\theta L_r}$ and gives rise to

different scalings depending on the characteristic lengths scales assumed. Two such assumptions have proven particularly popular, providing fodder for three decades of debates over the nature of plasma turbulent transport. The first of these corresponds to 'macro-turbulence' and makes the assumption that all length scales are proportional to the plasma size itself (e.g. the minor radius) and lead to

$\chi \propto \dfrac{T}{eZB} \propto A^0$. This diffusivity is called Bohm-like because has the same dependences as the classical Bohm diffusion coefficient [Bohm 1949, Spitzer 1960]. The Bohm diffusion coefficient is a

worst case estimate obtained by assuming $\delta_t = \omega_{ci}^{-1}$ and $\Delta_r = \rho_i$. We wish to emphasize here that despite their identical dependences on temperature and magnetic field, Bohm and Bohm-like diffusion belong to very different theoretical frameworks, the former making no reference to drifts, let alone drift waves and turbulence. GyroBohm scaling, $\chi \propto \dfrac{T}{ZeB}\dfrac{\rho_i}{R} \propto A^{1/2}$, follows from the assumptions $\Delta_r \sim \rho_i$, $L_\theta \sim \rho_i$ and $L_r \sim a \propto R$, as expected for quasi-isotropic ion scale drift wave turbulence, i.e. ion temperature gradient (ITG) and trapped electron mode (TEM) turbulence. Equivalently, gyroBohm scaling can be obtained from a mixing length estimate, $\chi \approx <\gamma/k_\perp^2>$, with $k_\perp \propto 1/\rho_i$ and the growth rate $\gamma \propto k_\perp v_d f(L_{Te}, L_{Ti}, L_n, \nu_{ei}, T_i/T_e ...)$ if the complex dependencies in f are ignored [Horton 1981, Waltz 1985, Horton 1999, Bourdelle 2016].

Early experiments were add odds with gyroBohm scaling not only in the context of isotope dependencies: Experiments in DIII-D L-mode deuterium plasmas where species resolved transport investigations were performed showed $\chi_i \propto \rho_i^{-0.5}$ i.e. opposite in sign to gyroBohm, while the electron diffusivity scaled as $\chi_e \propto \rho_e$ [Petty 1995]. GyroBohm scaling does remain the fundamental underlying scaling for both quasi-linear and non-linear gyrokinetic physics in the local, electrostatic, collisionless, flowless limit with adiabatic electrons, as shown in non-linear GYRO simulations [Pusztai 2011]. These have resulted in non-linear heat fluxes that do indeed closely follow the expected scaling, $Q/Q^H_{gB} \propto A^{-1/2}$. The result is consistent with Rosenbluth-Hinton zonal flows [Rosenbluth 1998], which have radial scales larger than the trapped ion widths and retain gyroBohm scaling of heat fluxes also in the non-linear saturated stage. However, as seen in advanced modelling and in experiment, the above mentioned neglected physics can modify the basic gyroBohm scaling beyond recognition.

The first mechanism discovered to be capable of causing deviations from gyroBohm scaling is most likely E×B shear flow stabilisation [Waltz 1998, Hahm 1995]. E×B shear flow may arise e.g. from sheared toroidal rotation due to momentum injection by neutral beam heating (NBH). It is also intrinsic to the formation of zonal flows [Rosenbluth 1998, Diamond 2005, Hahm 2013, Bustos 2015] which damp/regulate the turbulence level in its developed, nonlinear state. The mechanism leads to turbulence quenching when the rotational flow shear rate exceeds the growth rate of the instability. It was not initially invoked for explaining isotope effects, however we can see from a quasilinear estimate of ion heat diffusivity χ_i how an isotope dependence may arise from it. From $\gamma_{max}^i = \gamma_{max}^H A^{-1/2}$ and hence $\chi_{gB}^i = \chi_{gB}^i A^{1/2}$ it follows

$$\chi_i \propto \chi_{gB}^i \left(1 - \alpha \frac{\omega_{E\times B}}{\gamma_{max}^i}\right) = \chi_{gB}^H A^{1/2}\left(1 - \alpha \frac{\omega_{E\times B}}{\gamma_{max}^H} A^{1/2}\right) \qquad \text{(eq.1)}$$

where $\omega_{E\times B}$ is the shearing rate, which may arise from gradients of the toroidal velocity or from ion temperature gradients (see e.g. Ref [Ernst 1998]), γ_{max} is the growth rate of the fastest growing mode and α a parameter describing the strength of shear flow stabilisation. For $\alpha* = \alpha \omega_{E\times B}/\gamma_{max}^H = 0$, there is no stabilisation, for $\alpha* > 0.36$, $\chi_T < \chi_H$ as sketched in fig.1 and for $\alpha* = 0.58$ there is complete suppression for tritium, but not for hydrogen and deuterium (where H, D and T stand for hydrogen, deuterium and tritium respectively). Hence the E×B effect may lead to an isotope effect opposite to gyroBohm both for E×B resulting from sheared bulk rotation and via zonal flows [Bustos 2015]. It should hence be noted that deviations from gyroBohm scaling do not imply that the transport is not governed by ion scale turbulence (e.g by macro-turbulence if a Bohm-like scaling, $\chi_i \propto A^0$, is observed). We also note that in 'real world' situations, the simple picture of eq.1 is likely to be complicated by the fact that $\omega_{E\times B}$ itself, whether from zonal flows or externally imposed, is likely to also depend on the isotope mass.
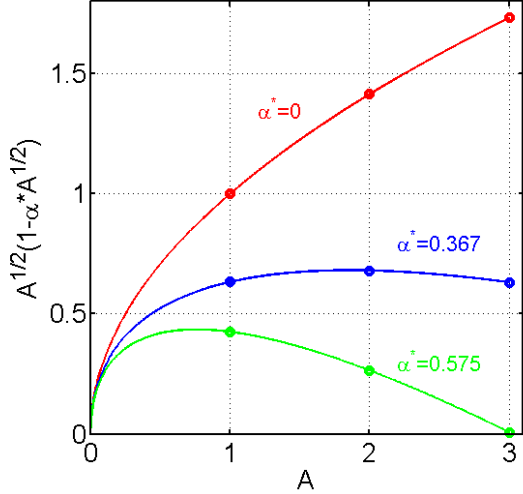
Fig.1. Sketch to illustrate eq.1. Isotope dependence of shear flow stabilisation for 3 values of $\alpha* =\alpha\omega_{E\times B}/\gamma_{max}$, assuming gyroBohm scaling for underlying transport ($\alpha*=0$)

E×B shear flow stabilisation was credited for stabilising turbulence in the H-mode edge transport barrier [Biglari 1988, Hinton 1991] and in enhanced core confinement regimes such as the H-mode pedestal, VH modes in DIII-D and TFTR supershots [Hahm, 1996]. In TFTR L-modes and supershots, E×B shearing was used to explain the not only improved confinement, but also the observation of stronger confinement improvement for D-T mixtures over pure D plasmas [Scott 1995, Ernst 1998]. However, with hindsight, other mechanisms, which were not yet discovered at the time, must have played a role too in these enhanced core confinement regimes. Analytical work by Hahm et al [Hahm 2013] with kinetic particles showed that finer scale zonal flows (narrower than the ion banana width) can lead to reduced transport with respect to gyroBohm scaling for the heavier isotopes. This was confirmed in non-linear simulations using the gyrokinetic code GENE [F. Jenko 2000, T. Görler 2011], which exhibited notable deviations from gyroBohm scaling in TEM and mixed TEM/ITG turbulent plasmas with $T_i/T_e=1$, with $Q^T/Q^T_{gB}/(Q^H/Q^H_{gB})\sim0.82$ [Bustos 2015]. The reduction of heat flux with isotope mass was attributed to a stronger zonal flow stabilisation of the turbulence at higher isotope mass, with $\omega_{E\times B}/\gamma_{max}$ increasing with isotope mass. A similar behaviour is observed when TEM turbulence is stabilised by electron-ion collisions: near marginality, the role of zonal flows in turbulence regulation is enhanced and this more strongly at high isotope mass [Nakata 2017]. This effects adds to the linear stabilisation of TEM by collisions which scales as $\nu_{eff} \sim \nu_{ei}/\gamma_0 \propto A^{1/2}$, where γ_0 is the collisionless growth and is therefore stronger at high isotope mass [Angioni 2018]. Nonlinear GENE [F. Jenko 2000, T. Görler 2011] simulations by one of the authors (M. Oberparleiter) in the course of the isotope effect investigations in JET [Maggi 2018, Weisen 2018] confirmed this mechanism is also active in ITG dominated turbulence and will be presented in detail later in the paper. A reversal of gyroBohm scaling has also been linked to the electron-to-ion mass ratio dependence of the non-adiabatic electron response when the turbulence is strongly influeced by the electron parallel dynamics (as for TEM and for the highly collisional plasma edge) [Belli 2019, Bonanomi 2019 *Nucl. Fusion* **59** 126025].

Electromagnetic effects can lead to an isotope effect as well through a non-linear process as demonstrated for an ITER case in DD vs DT. Whereas linear simulations do not show a departure from gyroBohm scaling, at high beta the ion heat flux decreases with increasing mass due to a non-linear interplay between zonal flows, electromagnetic effects and mass [J. Garcia et al 2017, PPCF]. Such a deviation from gyroBohm scaling is enhanced in plasma conditions of high beta and high E×B shearing, as expected in advanced tokamak scenarios with high NBH power. In the particular case of DD vs DT plasmas, the additional fast ion contribution from the alpha particles from DT reactions can further reduce the ion heat flux by fast ion electromagnetic stabilization resulting in considerable de-stiffening of the ITG mode, typically halving the ion heat flux for a given ion temperature gradient length [J. Garcia 2018]. The higher fast ion pressure in deuterium plasmas heated by energetic ions has lead to improved core confinement in a set of L-mode experiments in JET, with ³He minority ICRH in addition to NBH [N. Bonanomi *et al* 2019 *Nucl. Fusion* **59** 096030]. It is important to stress that a different fast ion contribution in different plasma species is not an inherent isotope effect. In the case of a comparison of D and DT plasmas such an effect, if not understood, may lead to erroneously

attributing the improved confinement in DT to a mass dependence.

Modelling of transport in the edge plasma and pedestal is still in its infancy, but deserves particular attention, as it sets the boundary conditions and via profile stiffness influences and often largely determines global confinement [Bateman 1999]. Strong ion mass effects have been obtained in electromagnetic gyrokinetic GENE simulations of L-mode edges in AUG and JET [Bonanomi 2019].The results show that edge turbulence is radically distinct from core turbulence. Electron parallel dynamics is important due to the high collisionalities at the edge, leading, in linear electrostatic simulations, to a stronger non-adiabatic electron response at low ion mass and to a lower R/L_{Te} threshold for hydrogen than for deuterium. This linear effect is also seen in non-linear simulations, resulting in a strong deviation from gyroBohm ($\chi_H \sim 2\chi_D$) already in electrostatic simulations. Due to the steep gradients, electromagnetic effects are also important despite the relatively low local thermal β. MHD-like electron drift waves are strongly destabilized even at low (with respect to core values) values of β_e. This destabilization especially affects modes with low wave numbers and is found to take place below the threshold in β_e expected from linear simulations [Bonanomi 2019]. This behaviour puts into questions the applicability in the edge plasma of the conventional approach of developing quasilinear models for describing transport. These novel results on the L-mode edge call for an extension of gyrokinetic modelling to the H-mode pedestal, which is found to be responsible for most of the isotope scaling of confinement observed in JET H-modes, as reported in section 5.

2.2 Operational effects

It is difficult and often impossible, to perform experiments in which an isotope is substituted for another, without changing any other plasma parameters. These operational effects can obscure the intrinsic transport effects, making their unambiguous identification difficult. Neutral beam heating (NBH) and ion cyclotron resonance heating (ICRH) confer heat to electrons and ions in proportions which depend on the background ion as well as on the fast particle masses and energies. Moreover, no ICRH method can be applied indistinctly to plasmas with arbitrary isotopes or isotope mixtures. The power, torque and particle sources by NBH depend on both beam ion isotopes and hence also on the background plasma, as the general preference is to use the same species for NBH as for the main plasma. This warning can be extended to a comparison of D and DT plasmas, as the latter, unlike the former, will produce alpha particles which are potentially capable of reducing ITG turbulence by electromagnetic effects [J. Garcia et al 2018, PPCF].
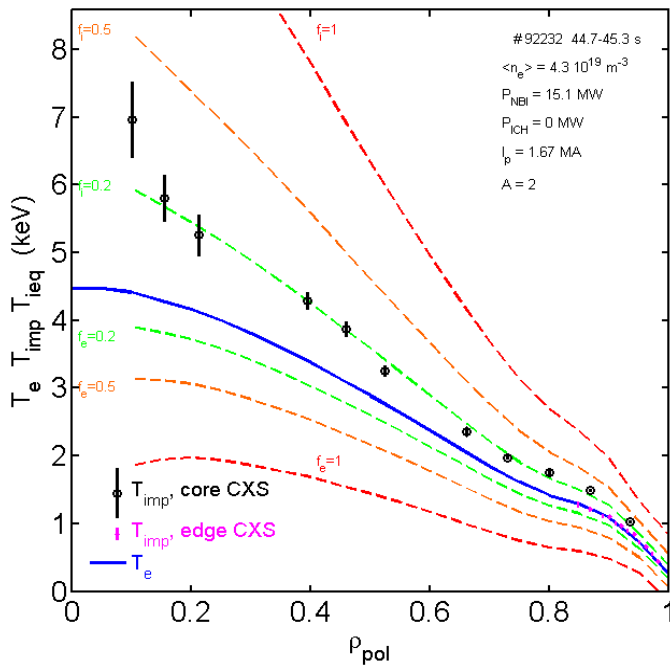
Equipartional energy exchange between ions and electrons, as well as between ions, depends on the plasma isotopes, affecting the ion and electron power balances and hence transport. Such a case was reported from a comparison of ECH heated L-mode in hydrogen and deuterium in ASDEX-upgrade [Schneider 2017]. The two discharges achieved the same electron temperature profiles and nearly the same ion temperature profiles, although the hydrogen discharge required 1.4MW of ECH power for only 1.06MW for the deuterium discharge. A species resolved power balance calculation revealed that the electron heat flux was unchanged, however the ion heat flux was 1.5-2x larger due to stronger electrons-ion thermal equipartition for the hydrogen case. The additional heat flux had virtually no effect in the ion temperature profile because of profiles stiffness as modelled using a critical gradient model [Garbet 2004]. In JET Ohmic discharges too, the difference in electron-ion equipartion between hydrogen and deuterium was found to be a key parameter in understanding the observed somwhat larger ion heat diffusivity in hydrogen [Delabie 2017].

The edge neutral penetration is deeper for the lighter species, which is expected to help fuelling for the lighter species. Cryopumping is more effective for the heavier hydrogenic species, affecting divertor

and edge conditions. Orbit losses are reduced for the lighter species. Some effects are not understood, as for instance the cause of the much higher particle transport in the edge of hydrogen H-modes in JET-ILW [Maggi 2018] and ASDEX-upgrade [Laggner 2017] (but not in JT-60U [Urano 2013]), which affect overall confinement. The planned DT experiments in JET have prompted a multi-campaign investigation of isotope effects in view of understanding the physics and in order to provide better extrapolation to the performance to be expected from the discharges under preparation for DT. Many of the results in hydrogen and deuterium plasmas have already been reported and will not be repeated here [Maggi 2018, Maggi 2019].

3. Diagnostics and data analysis for JET-ILW isotope studies

The most important diagnostics used in this study were the two Thomson scattering systems, HRTS [Frasinetti 2012] and LIDAR [M. Maslov 2013] for electron temperature and density profiles. Unless otherwise indicated, we have used the HRTS system because of its better spatial resolution. Charge exchange spectroscopy (CXS) data for T_i and toroidal angular frequency ω_ϕ are available for about half of the dataset [Giroud 2008]. Uncertainties on T_i derived from CXS on impurity lines are significantly higher in JET-ILW due to reduced carbon levels and the appearance of multiple tungsten "nuisance" lines, than they were in JET-C. The electron temperatures in these discharges were also generally too low for reliable ion temperature measurements using X-ray crystal spectrometry for the a $^{59}Ni^{26+}$ K-shell at X-ray line at 1.6Å [Schumack 2014]. Consequently all profile data were subjected to a thermal "equipartion test" in order to filter out any data points (about 12% of cases) where the calculated ion-to-electron equipartition power p_{ie} (which is proportional to T_i-T_e) integrated over the volume $Q_{ie}=\int p_{ie}dV$ exceeded the integrated deposited ion source power $Q_{is}=\int p_{is}dV$. A useful way of testing equipartition is to compare the measured ion temperatures to a set fictional ion temperature profiles, dubbed "equipartition ion temperatures", consistent with a certain fraction f_i of the source power being transferred to the electrons by equipartition [Weisen 2020]. In other words, $T_i(f_i,\rho)$ refers to the ion temperature profile required to have that $Q_{ie}=f_i\times Q_{is}$ and is calculated on the basis of the measured electron density and temperature profiles and the ion heat deposition profile. The relevant temperature profiles are shown for one example in fig.2, for f_i=0.2,0.5 and 1. For illustration purposes, we have chosen a sample with one of the highest measured ratios of T_i/T_e. An analogous power balance can be calculated for electrons (f_e-labelled profiles in fig.2, although not relevant to this case), if net equiparion is from the electrons to the ions.

Fig.2 Profiles from hydrogen pulse 92232: Electron temperature T_e (blue), the measured impurity temperatures from the main CXS system (black sybols) and the edge CXS system (magenta symbols at ρ_{pol}>0.8). The broken green, orange and red lines labelled f_i and f_e are 'equipartition ion temperatures' and are explained in the main text.

Clearly f_i≥1 is unphysical, as the ions would have zero or negative net heat flux. Fig.2 also shows the CXS impurity temperatures simultaneously inferred from Ne and C in black,

the former having been introduced as a tracer (with $n_{Ne}/n_e \sim 0.2\%$) to improve the measurements. With collisional ion heating, as here with NBH, the main ion temperatures T_{main} can can be somewhat lower than the impurity temperature [Weisen 2020]. In the majority of cases in this dataset (T_{imp}-T_{main})/T_{main}<0.03 in the plasma core and (T_{imp}-T_{main})/T_{main}<0.01 near the plasma boundary and is insignificant for this study.

The fact the T_{imp} profile in fig.2 is close to the "equipartition ion temperature" calculated for f_i=0.2 is not a coincidence [Weisen 2020, H. Weisen 2018] and is used to improve on the assumption $T_i = T_e$. When the JET isotope experiments were first analysed [Maggi 2018], ion temperature measurements were not available and $T_i = T_e$ had to be assumed. For this paper, ion temperatures from CXS for about half the discharges presented became later available. The power balance analysis allows this assumption to be replaced by the assumption $T_{main}(\rho) = T_{ieq}(f_i=0.2,\rho)$, i.e. by adopting $T_{ieq}(f_i=0.2, \rho)$ as a proxy for T_{main} for the purpose of improved confinement regressions, using the complete experimental dataset. The data analysis for the global confinement in JET discharges presented in sections 4 and 5 was performed using the JETPEAK database, presented in appendix 1 of ref [Weisen 2020].

Isotope ratios were primarily based on line intensity ratios from high resolution Balmer-alpha spectroscopy, using a set of several vertical viewing lines passing through the divertor [Neverov et al 2017]. Residual gas analysis in the sub-divertor, based on Penning gauge spectroscopy [U. Kruezi 2012], was also available. These isotope fractions $n_D/(n_D+n_H)$ and $n_H/(n_D+n_H)$ from the two diagnostics were found to agree within a few percent. The majority of the JET results presented here are in 'pure' isotope plasmas, i.e. the external gas fuelling and the NBH used the same isotope. In these conditions the purity of that isotope was typically better than 97%. In mixed H/D plasmas the core isotope composition was inferred from the measured DD neutron rates as explained in section 5.4 and in refs [Maslov 2018, King 2020, King 2017].

4. Isotope dependence of global confinement in JET-ILW L-modes

A dataset of 20 samples was obtained by NBH power scans in hydrogen and deuterium with B_T=3T, I_p=2.5 MA, $<n_e> \cong 3.1 \times 10^{19} m^{-3}$, 1.5MW$\leq P_{NBI} \leq$9.5MW, B_T is the toroidal magnetic field at the vessel centre, I_p the plasma current, P_{NBI} the NBH power and $<n_e>$ is the volume averaged density. The experiment was intended to be carried out at constant density, however this was successful only within $\pm$10%. The divertor strike points were placed on the vertical tiles for highest H-mode power threshold in order to maximise the L-mode domain in these experiments. It was previously shown that these discharges are dominated by ITG turbulence [Maggi 2018].

The thermal stored energy is calculated as

$$W_{th}=1.5e\int(n_e(\rho)T_e(\rho)+n_i(\rho)T_{ieq}(f_i=0.2,\rho))dV(\rho) \qquad (eq.2),$$

where n_i is estimated as

$$n_i= n_e-(Z-1)n_Z=n_e(1-(Z_{eff}-1)/Z), \qquad (eq.3)$$

The electron density in JET L-modes is easily controlled via the gas puff rate. JET-ILW plasmas are of high purity with the bulk of the data presented having 1.05<Z_{eff}<1.6, as inferred from visible Bremsstrahlung measurements for this L-mode dataset. As a result, errors on n_i/n_e inferred by assuming a single impurity species are small (<10%). Fig.3 shows a regression for the thermal stored energy assuming $T_i(\rho)=T_{ieq}(f_i=0.2,\rho)$:

$$W_{th} \propto P^{0.35\pm0.02}A^{0.18\pm0.02}<n_e>^{0.71\pm0.11} \qquad (eq.4)$$

where P is the total deposited power.

The lower legend of the figure shows, from left to right, the standard deviation σ of the regression, the variable names, the fit coefficients (b, the exponents of the power law), their errors for a 10% confidence interval (δb), the statistical significance STS (b/δb) and the normalised statistical relevance

STR, which for every regressor i is given by $b_i \cdot \sigma_i / \sigma_t$ where σ_i is the standard deviation for regressor i in the dataset and σ_t is the standard deviation of the target variable [Kardaun 2005]. Hence the STR quantifies to what extent a particular regressor contributes to the variations of the target variable.
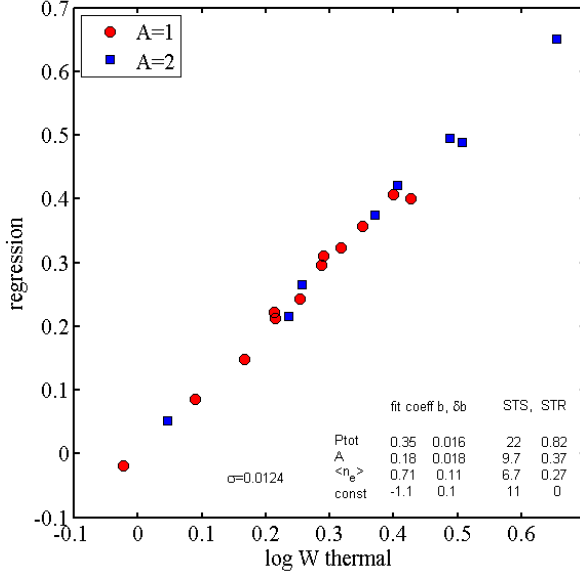

	fit coeff b, δb		STS, STR	
Ptot	0.35	0.016	22	0.82
A	0.18	0.018	9.7	0.37
$<n_e>$	0.71	0.11	6.7	0.27
const	-1.1	0.1	11	0

σ=0.0124

Fig.3: Regression of thermal stored energy expressed in MJ in L-mode dataset as in eq.4. P_{tot} is the total power, A is the isotope mass, $<n_e>$ the volume average density and σ the standard deviation. The legend is explained in the main text.

The uncertainties in the measured density and temperature profiles are typically of order 10%. Assuming $T_i(\rho)=T_{ieq}(f_i=0.2,\rho)$, the core ion temperatures exceed the electron temperatures by 3% (at $P_{NBI}=3MW$) to 8% (for $P_{NBI}=9MW$) in deuterium and by 1% (at $P_{NBI}=3MW$) to 5% (for $P_{NBI}=9MW$) in hydrogen. A comprehensive study [Weisen 2020] shows that for those cases where T_i is available from CXS, $f_i>0.4$ is very rare and the few such cases observed may well be the result of measurement errors. Hence we consider a core a core ion temperature exceeding the electron temperature by 16% as the upper error bar for $P_{NBI}=9MW$. Moreover, the relative difference between $T_{ieq}(f_i,\rho))$ and T_e becomes very small (a few %) near the LCFS, which contributes significantly to W_{th} to due to the large volume. Altogether, the usage of $T_{ieq}(f_i=0.2,\rho)$ in eq.2 brings an improvement over the assumption $T_i=T_e$, albeit admittedly, a modest one. Z_{eff} in these low power discharges is near 1.15 for $P\approx3MW$, rising to between 1.2 and 1.45 for $P\approx9MW$, with an error estimated from the data dispersion to about 0.1. This corresponds to an error in $n_i=n_D+n_H+n_{Be}$ of less than 3%, which therefore contributes little to the overall errors on W_{th}. Finally we should note that the errors on W_{th} propagate only partly to the scaling exponents, as systematic over- and underestimates by constant factors, which are most difficult to quantify, have no effect on the scaling exponents.

The inferred difference in T_i/T_e between high and low power plasmas indicates that stronger electron-ion equipartition, as in [Schneider 2017] and the stronger direct electron heating by NBH play a role in the scaling. If we simply assume $T_i=T_e$ the mass scaling is slightly weaker:

$$W_{th2} \propto P^{0.32}A^{0.15}<n_e>^{0.75} \qquad \text{(eq.5)}$$

If the thermal energy is inferred from the plasma energy W_p provided by unconstrained EFIT [General Atomics EFIT website] equilibrium reconstruction and the perpendicular and parallel fast particle contributions $W_{f\perp}$ and $W_{f//}$ as

$$W_{thMHD}=W_p-1.5W_{f//}-0.75W_{f\perp} \qquad \text{(eq.6)}$$

the mass exponent is regressed as

$$W_{thMHD} \propto P^{0.49}A^{0.14}<n_e>^{0.3} \qquad \text{(eq.7)}$$

$W_{f//}$ and $W_{f\perp}$ used in eq.5 are the parallel and perpendicular fast particle stored energies and were obtained from the PENCIL [Challis 1989] NBH code. Eq. 6 can be inferred from the effect of pressure anisotropy on the equilibrium [Cooper 1982, Fitzgerald 2015]. In all of the above regression, the mass exponents are close to the L-mode exponents published the ITER physics basis [ITER Physics Basis 1999] and to the one previously reported for JET-ILW [Maggi PPCF 2018].

The difference in exponents for P and $<n_e>$ between eq.7 and eq.5 is likely due to it being poorly constrained due to the smallness of the variations of $<n_e>$ (±10%). Because of the limited variations in $<n_e>$, the density exponents are not significant. Although the density dependence is not the subject of this study, it raises the question whether the weak mass dependence itself may be biased by the small

variations in density in the dataset and the correlation between density and isotope mass. The correlation coefficients between these parameters is +0.39, which is not negligible. We therefore have repeated the above regressions (eqs.4, 5, 7) leaving out the density with the results $W_{th} \propto P^{0.39\pm0.05}A^{0.23\pm0.05}$, $W_{th2} \propto P^{0.36\pm0.05}A^{0.2\pm0.05}$ and $W_{thMHD} \propto P^{0.5\pm0.03}A^{0.17\pm0.03}$. We note that, as expected, the exponents for A are now higher, but only slightly so, as the isotope dependence so obtained incorporates both the intrinsic isotope dependence and the effect of the correlation with the density. The mass exponents obtained without taking into account the density variations should therefore be considered as upper limits. We conclude that the (unwanted) density variations in the dataset do not alter our conclusion and that the isotope dependence for energy confinement in L-mode is weak, with a mass exponent estimated to be in the range 0.14-0.18, as indicated by regressions eq.4,5 and 7.
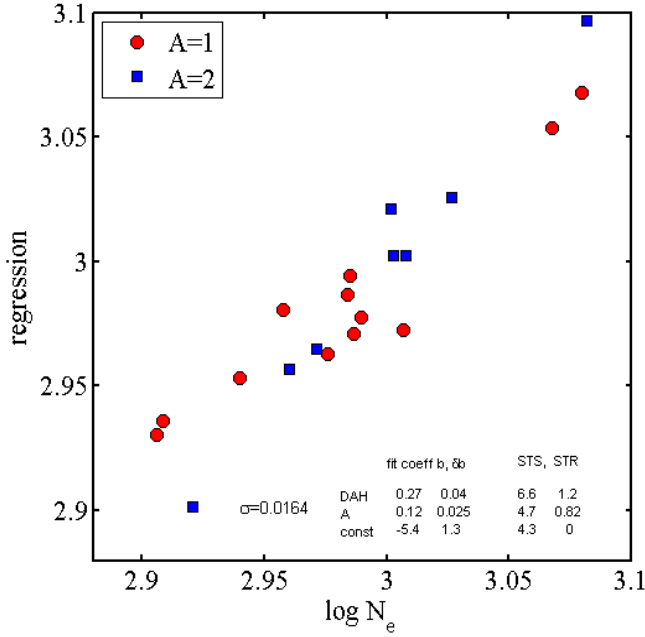
The total particle content $N_e=\int n_e dV$ is best regressed with A and a proxy for the edge particle source Γ given by the Balmer-alpha emission measured along a horizontal line in the vessel midplane, as seen in fig.4.

$$N_e \propto A^{0.12}\Gamma^{0.27} \qquad (eq.8)$$

Fig.4. Regression of total particle content in units of $1\times10^{19}m^{-3}$ in L-mode dataset as in eq.8. DAH stands for D-α emission along a horizontal line of sight and used as a proxy (in a.u.) for Γ in eq.8.
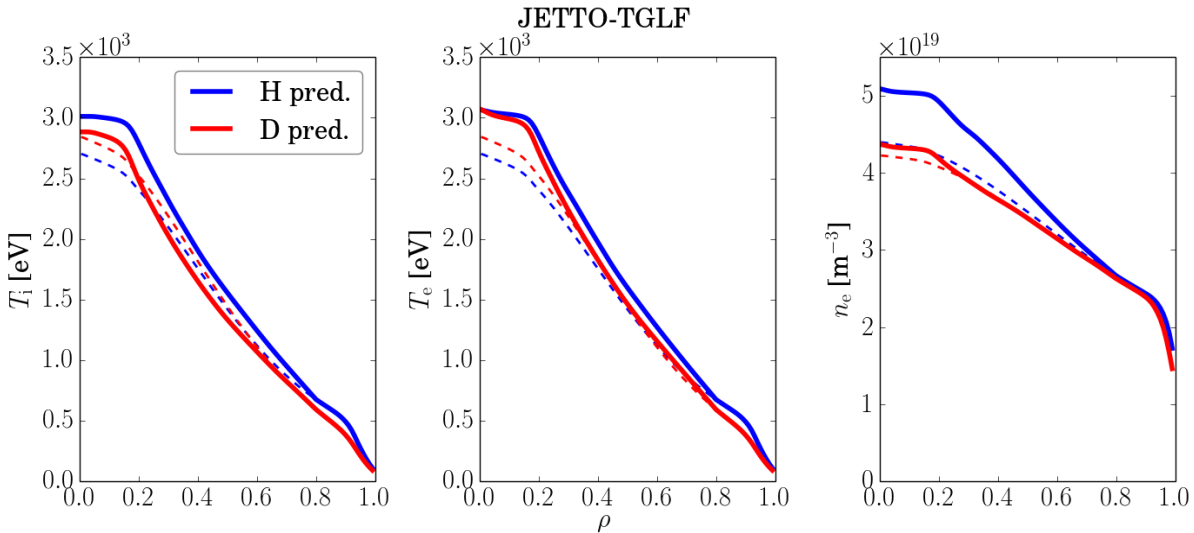

Fig.5 Experimental (dashed lines) and simulated (continuous lines) profiles for hydrogen (blue) and deuterium (red) L-mode discharges with the same stored energy.
Hydrogen #91450, P=4.4MW, $\tau_{E,exp}$=0.235s, $\tau_{E,pred}$=0.294s
Deuterium: #89723, P=3.2MW, $\tau_{E,exp}$=0.283s, $\tau_{E,pred}$=0.289s

While the density variations in the dataset are small (±10%), the regressions are constrained by the variations of isotope mass (factor 2) and of Γ (factor 3). The observation that the energy and the particle confinement have similar isotope scaling, within errors, is unlikely to be a result of chance, as turbulent transport theory generally predict a close relationship [C. Bourdelle 2018]. A hydrogen/deuterium pair from the above set with nearly the same thermal stored energy (1.2MJ) and line averaged density ($3.1 \times 10^{19} \text{m}^{-3}$) with respectively 4.4MW (hydrogen) and 3.2MW (deuterium) NBH, was predictively modelled under conditions of imposed heat flux using JETTO with the TGLF SAT-1 quasilinear transport model, which is based on non-linear turbulence simulations based on the GYRO code [Staebler et al 2007, Staebler et al 2017]. We must note here that this version of TGLF is based on simulations in deuterium only. The boundary conditions, imposed at ρ=0.85, were taken from the experimental data. Predicted and experimental profiles, shown in fig.5, are in good agreement for deuterium, less so for hydrogen, for which temperature and density are overpredicted [J. Garcia et al 2019 Nucl. Fusion 59 086047]. ITG modes are dominant in the core and the inclusion of E×B shear from NBH driven toroidal rotation in these cases does not lead to an improvement of deuterium confinement relative to hydrogen. We note however, from the available CXS data, that the toroidal rotation and it's shear in hydrogen were 10-30% larger in hydrogen than in deuterium. The predictions yield nearly the same global confinement time for both species ($\tau_{E,pred}$ =0.294 for hydrogen, 0.283 for deuterium), i.e. neither gyroBohm scaling, nor weak anti-gyroBohm scaling, as indicated by the experimental results. This is interpreted as resulting from profile stiffness (high resilience of R/L_T to changes in the heat flux) which is seen in the experiment [Maggi 2018] and is borne out in the simulations. Results may change in future versions of TGLF trained on both deuterium and hydrogen, although they would still remain constrained by the boundary conditions.

These experiments were also modelled using the gyrokinetic code GENE [F. Jenko 2000, T. Görler 2011]. The simulations have shown that the E×B shearing rate, the effects of collisions and of trapped electrons lead to deviations from the expected gyroBohm scaling in ITG dominated plasmas. Analyses were also performed for the above L-mode discharge #91450 (hydrogen) by artificially changing the mass from 1 to 2 [J. Garcia et al 2019 Nucl. Fusion 59 086047]. With the above effects included, the ratio Q_D/Q_H is about 0.85. However, Q_D/Q_H progressively increases by removing these effects one by one, recovering gyroBohm scaling ($Q_D/Q_H = \sqrt{2}$) when all are removed. E×B shearing and the effect of collisions are found to be the largest contributors to the deviations from gyroBohm scaling.

In a separate experiment, a H/D pair of L-mode discharges matched for being identical in the dimensionless parameters $\rho*$, β, $\nu*$ and q, was created [Maggi 2019]. This was achieved at I_P/B = 2.5MA/3.0T in D and 1.48MA/1.78T in H, q_{95} = 3.4, δ = 0.2, with strike points on divertor vertical targets. In order to keep the $\rho*$, β, $\nu*$ and q profiles fixed when varying the isotope mass, the plasma parameters must be scaled as $I_P, B_T \propto A^{3/4}$; $n \propto A$ and $T \propto A^{1/2}$ [Cordey 2000]. The experiments achieved scale invariance, i.e. the normalised profiles were identical. The same scale invariance principle also predicts that $\omega_{ci}\tau_{Eth} \propto B\tau_{Eth}/A$ is invariant under this scale invariant transformation. In these experiments $B\tau_{Eth}/A$ was *0.27 T*s for the hydrogen case and *0.28 T*s for the deuterium case, i.e. they were the same, within errors, in both plasmas. These identity experiments also confirm that $\rho*$, β, $\nu*$, q are the only significant parameters governing heat transport in these L-mode plasmas. We note that the equality of $B\tau_{Eth}/A$ (or locally of $A\chi/B$) at fixed $\rho*$, β, $\nu*$, q does not, on it's own, qualify the nature of the underlying transport (gyroBohm, Bohm-like or other) as can be achieved with a scan of $\rho*$ [Petty 1995, Cordey 1996]. Predictive modelling with JETTO-TGLF of the isotope identity pair, with boundary conditions imposed at ρ=0.8, is in very good agreement with experiment for both isotopes, for both the particle and energy transport. The reader is referred to ref [Maggi 2019] for details.

5. Isotope dependence in JET-ILW type I ELMy H-modes

Due to the limited NBI power in hydrogen (~10MW), H-mode operation at a unusually low toroidal field for JET was necessary. A so-called "corner-corner" configuration, with strike points near the divertor pumping ducts was chosen for best density control and confinement for most of the discharges. The dataset size is 171 samples in total with subsets at B_T=1T, I_p=1MA ($q_{95} \cong 3$) and B_T=1.7T, I_p=1.4MA ($q_{95} \cong 3.7$), a few samples at 1.7T, 1.7MA in D only. Deuterium beams were used to heat the deuterium plasmas and hydrogen beam were used to heat the hydrogen plasmas. The power range in deuterium was 3.5MW $\leq P_{NBI} \leq$ 16.6 MW (only NBI) and in hydrogen 3 MW $\leq P_{NBI}$ $\leq$ 10.4MW, $0 \leq P_{ICRH} \leq$ 6.2MW. The ICRH power, provided by 2nd harmonic hydrogen heating, was necessary in some hydrogen discharges to access type I ELMy H-modes at the higher field on 1.7T. The experiments consisted mostly in systematic scans of the external gas puff rate and power scans. Many of the lower power hydrogen H-modes were in type III ELMy H-mode and were excluded from the dataset. The experimental conditions of these experiments were presented in greater detail in ref [Maggi 2018].

It turned out to be impossible to produce pairs in hydrogen and deuterium with matched density, except in a few cases, because of the much lower particle confinement for hydrogen H-modes. Fig.6 a) shows the total particle content $N_e=\int n_e dV$ versus the Balmer alpha emission along a horizontal viewing line. There is little overlap in the density ranges obtained in hydrogen and deuterium. Gas puff rates several times larger in hydrogen were often necessary to obtain similar densities. In deuterium H-modes, the gas puff rate did not allow the density to be controlled, unlike hydrogen plasmas, where increased puff rates (and edge particle sources, as seen in fig.6a) did allow increasing the density. The temperatures obtained were similar in both species. This behaviour is in stark contrast to that observed in JT-60U, where the same densities were easily obtained, but temperatures in hydrogen were lower than in deuterium [Urano 2913]. Fig.6 b) shows that the ratio of the fast ion stored energy from NBH, calculated using the PENCIL code [Challis 1989], scales fairly linearly with the NBH power divided by the particle content P_{NB}/N_e , however in hydrogen the fast ion contribution is lower, which can be understood from the scaling of the slowing down time $\tau_{slow} \propto T_e^{3/2}/(A n_e)$. The core ion to electron temperature ratio T_i/T_e at ρ=0.3 , estimated as $T_{ieq}(f_i$=0.2,$\rho)/T_e(\rho)$, increases up to near 1.4 with P_{NB}/N_e, as seen in fig.5c and is lower in hydrogen plasmas. The figure also shows available CXS measurements, marked with + signs (red of hydrogen, blue for deuterium). They show a similar increase of T_i/T_e with P_{NB}/N_e, although there appears to be no systematic difference between the two
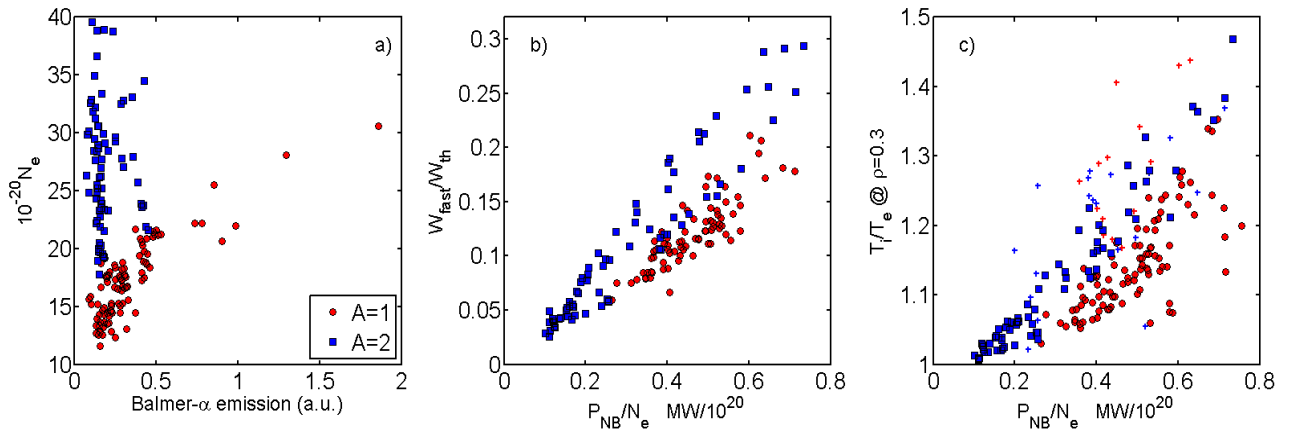
species.

Fig.6. a) Plasma electron content vs Balmer-α emission as proxy for edge source, b) Ratio of fast ion stored energy to thermal stored energy vs NBH power per particle, c) Core T_i/T_e ratio vs NBH power per particle. Full symbols for T_i=$T_{ieq}(f_i$=0.2,ρ=0.3), + signs for T_i from CXS.

As good CXS measurements are only available for less than half of the data, we use $T_{ieq}(f_i=0.2,\rho)$ for evaluating the ion contribution to the confinement time. For most of the cases where CXS measurements are available $T_{ieq}(f_i=0.2,\rho)$ provides a good fit to the measured ion temperatures in this dataset, for both hydrogen and deuterium, as can be seen in fig.5 of ref [H. Weisen 2018]. We keep in mind that the uncertainties in T_i may contribute to several percent of error in global confinement time.

**5.1 Global thermal confinement in type I ELMy H-mode**

The thermal stored energy is calculated as in eq.2. Unlike what is the case for L-modes, the electron density in deuterium H-modes is essentially uncontrollable using gas puffing [Maggi 2015, Urano 2016, M. Maslov *et al* 2020]. We therefore here avoid $<n_e>$ as a regression parameter. Regressions including the density have been presented in [Maggi 2018, Weisen 2018], with similar results for the ion mass scaling. Instead, we use the Balmer-α radiation along a horizontal line as a proxy for edge fuelling. The intensity of Balmer-α emission scales with the gas puff rate roughly within a factor 2, over a factor of 20 over variation in the dataset, however better regressions are obtained with the the Balmer-α emission than with the gas puff rate. Satisfactory regressions using the divertor Balmer-α radiation or the gas puff rate are also obtained, however the Balmer-α radiation along a horizontal line provides the regressions with the lowest standard deviation.

The regression for W_{th} is shown in fig.7 and given below:

$$W_{th} \propto A^{0.53 \pm 0.05} P^{0.63 \pm 0.04} I_p^{0.83 \pm 0.08} \Gamma^{-0.17 \pm 0.04} \qquad \text{(eq.9)}$$

The standard deviation of this regression is 0.09. A very similar result is obtained if we regress for the thermal energy inferred from W_{MHD} as in equation 2 :

$$W_{th} \propto A^{0.48 \pm 0.05} P^{0.67 \pm 0.04} I_p^{0.86 \pm 0.09} \Gamma^{-0.2 \pm 0.03} \qquad \text{(eq.10)}$$
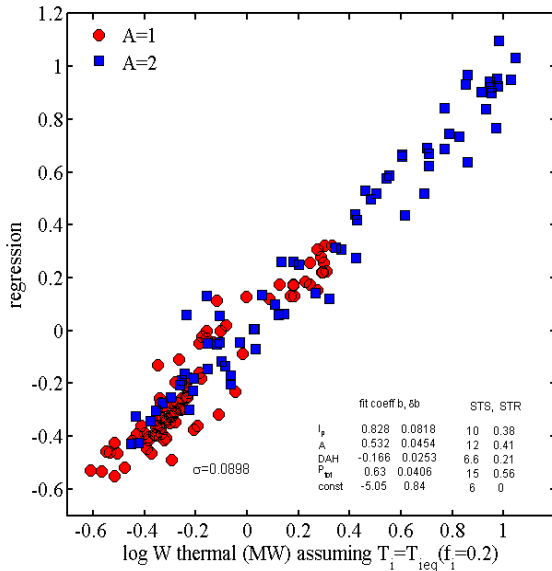
with a standard deviation of 0.094. (Regression in eq.10 is too similar to eq.9 to deserve its own figure).

Fig.7. Regression of the thermal confinement time in MJ correponding to eq.9. P_{tot} is the total power, A is the isotope mass, $<n_e>$ is the volume average density and σ the standard deviation. The legend is explained in the main text in section 4.

These scalings have a slightly stronger isotope dependence than reported in [Maggi 2018], which found $W_{th} \propto A^{0.4}$ using the plasma density rather than a measure of gas fuelling and assuming $T_i = T_e$. The scaling is significantly stronger scaling than in JET-C [JET Team 1999, Saibene 1999] and in the IPB(y,2) ELMy H-mode scaling ($W_{th} \propto A^{0.19}$) [ITER Physics Basis 1999]. A recent broad survey of H-mode confinement in JET, with 867 JET-ILW samples, including deuterium (the majority) and hydrogen plasmas also reports a strong isotope scaling in JET-ILW, with mass exponents in the range 0.35 to 0.43, depending on the choice of regression variables and data subsets [Maslov 2020]. In that study, the thermal stored energy was inferred from the diamagnetic energy which is based on external magnetic measurements, corrected for the perpendicular fast ion energy content. Interestingly, that study also finds that the

mass exponents are somewhat higher when a measure of gas fuelling is used instead of the plasma density. Altogether, this paper and refs [Maggi 2018, Maslov 2020], show that isotope scaling of thermal energy confinement in JET-ILW is robust to the choice of data sets and regression variables.

The normalised hydrogen and deuterium temperatures are similar, regardless of conditions. In fig.8 we show ∇T_e as function of T_e for ρ_{pol}=0.8 and 0.55. As the HRTS system suffered a miscalibration at 3 channels near the pedestal top for part of the data, we show this using data from the LIDAR Thomson scattering system. There is no discernible systematic difference in $\nabla T_e / T_e$ between the two species, nor for the different heat fluxes, which span a factor 9 at ρ=0.55 (fig.8a). In the meaning of stiffness as defined in ref [Garbet 2004], we see no evidence for a difference in stiffness between the two species, as already stated in [Maggi 2018].
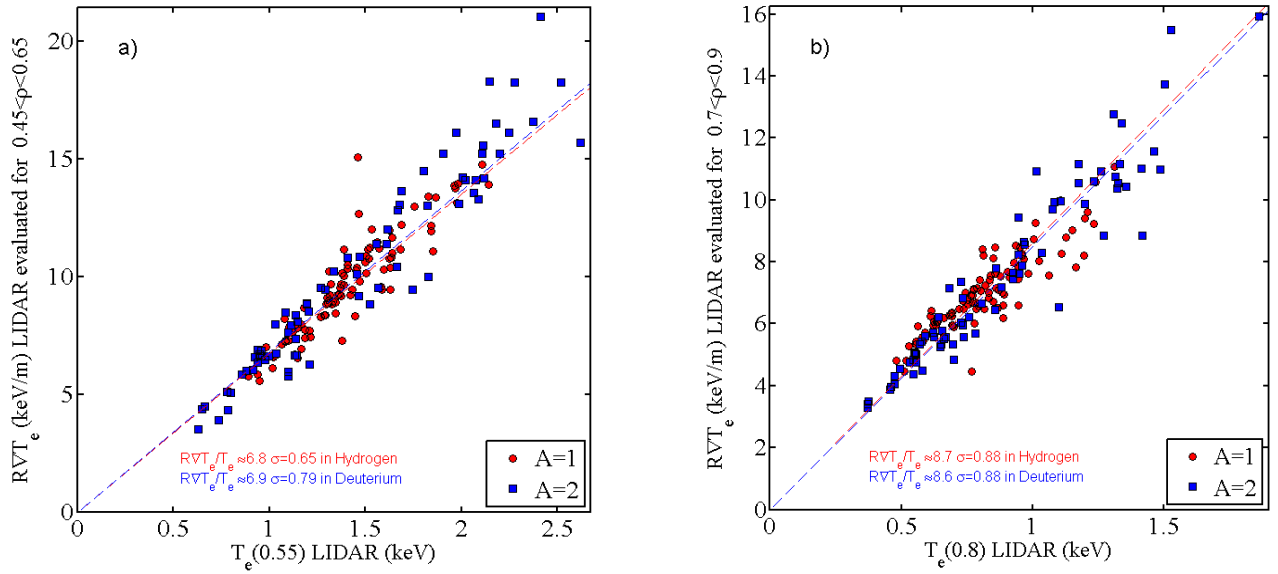

Fig.8. ∇T_e as function of T_e for a) ρ_{pol}=0.55 and b) ρ_{pol}=0.8. The dashed lines correspond to the averages of $R\nabla T_e/T_e$.
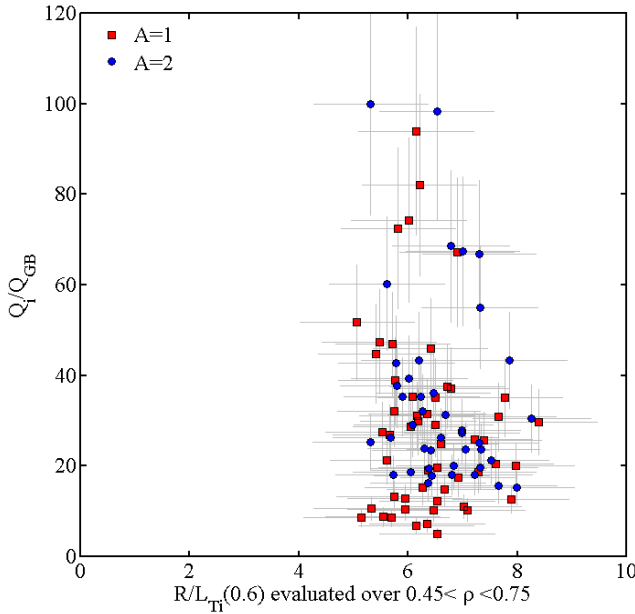

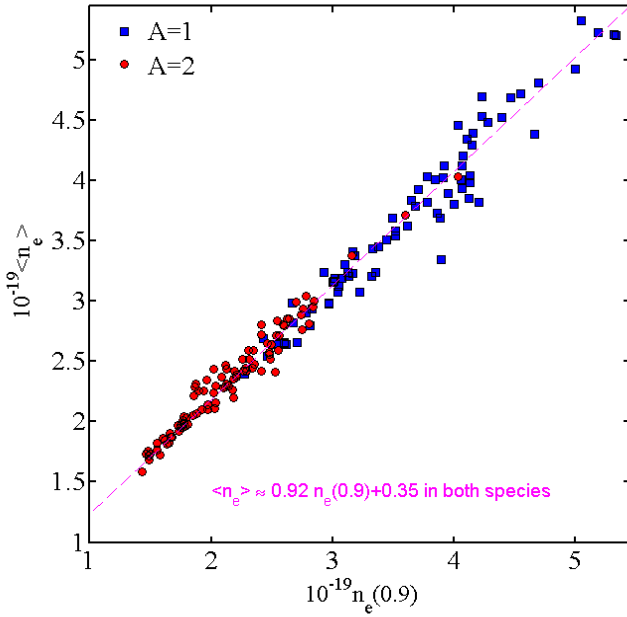*Fig.9 Ion heat flux in gyroBohm units vs normalised ion temperature gradient at ρ=0.6.*

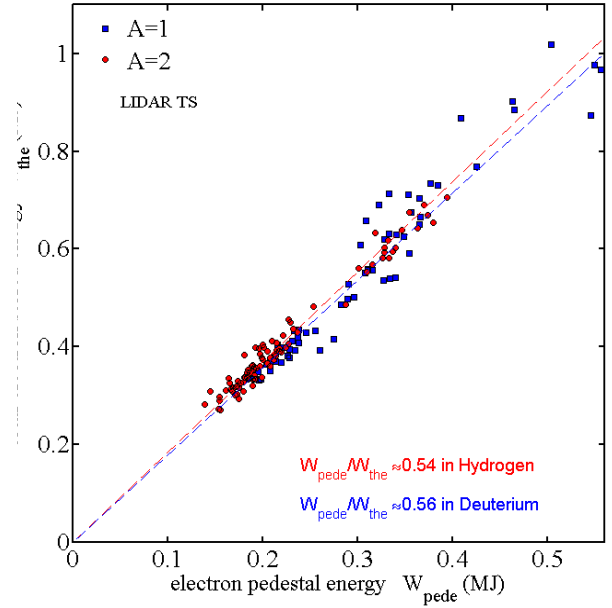14

Fig.10. Scaling of average density
with pedestal density

Fig.11 Proportionality of global and pedestal
stored energies

When normalised to the gyroBohm heat flux defined as $Q_{gB}=(Am_p)^{0.5}n_e(eT_i)^{2.5}R/L_{Ti}/(e^2B^2R_{geo}^2)R_{geo}/L_{ref}$ [W/m^2] [Garbet 2004], the range of ion heat fluxes in the dataset is even larger, as seen in fig.9 for $\rho=0.6$ as function of R/L_{Ti}. For this calculation we adopted $L_{ref}=R_{geo}$ as the reference scale length, assumed the effective surface for the calculation of the heat flux to be $S_{eff}=dV/dr$, with V the plasma volume, $r=(R_{max}-R_{min})/2$ and $R_{geo}=(R_{max}-R_{min})/2$, R_{max} and R_{min} being the maxima and minima of the flux surfaces at the plasma mid-plane. Although errors on the normalised heat flux and on R/L_{Ti} are large, we see that the measured gradients are mostly in the range range $5<R/L_{Ti}<8$ for both isotopes over a range of normalised heat fluxes, Q_i/Q_{gB}, of a factor 20. No dependence of Q_i/Q_{gB} on R/L_{Ti}, nor on the isotope is discernible. A possible species dependence, as reported in [Urano 2013], is likely to be obscured by a combination of experimental errors and of unresolved dependences of the critical gradient R/L_{crit} [Garbet 2004] on the wide range of plasma conditions in the dataset.

The density profiles of hydrogen and deuterium plasmas are remarkably similar too. The volume average density can be regressed as $<n_e>=0.92n_e(0.9)+0.35\times10^{19}$m^{-3} for both species, as seen in fig 10. (This implies that plasmas with lower density have somewhat more peaked density profiles). Together with the similarity of temperature profiles, this implies that the global electron energy is proportional to the electron energy at $\rho_{pol}=0.9$, which we take as a proxy of the pedestal electron energy (fig.11). The ratios of the pedestal to global stored electron energies for both species are well within error bars, $W_{pede}/W_{th}\approx0.56$ in deuterium and $W_{pede}/W_{th}\approx0.54$ in hydrogen. Hence, to within measurement errors, the species related differences in electron stored energy are attributable to differences in the pedestal. Ion temperatures are less stiff as T_i/T_e increases with $P/<n_e>$ more strongly in the core than nearer the pedestal top. Assuming $T_{ieq}(f_i=0.2,\rho)/T_e(\rho)$, this increase would be stronger for deuterium than for hydrogen as seen in fig.6c, contributing, albeit very modestly, to better global confinement in deuterium. Unfortunately accurate core ion temperature measurements, not available at this time, are required for backing up this conjecture.

5.2 Momentum confinement in type I ELMy H-mode

Fortunately the errors on angular velocity determined from CXS are lower than those on T_i and measurements are available for about half of the H-mode dataset. The maximum torque in the dataset was 20 Nm in deuterium and 12 Nm in hydrogen at the maximum NBH powers available. The global momentum ranged up to 4.7 Nms in deuterium and 1.8 Nms in hydrogen. Global angular momentum in hydrogen plasmas is considerably lower than in deuterium plasmas due to the lower NBH torque, the lower density and confinement.
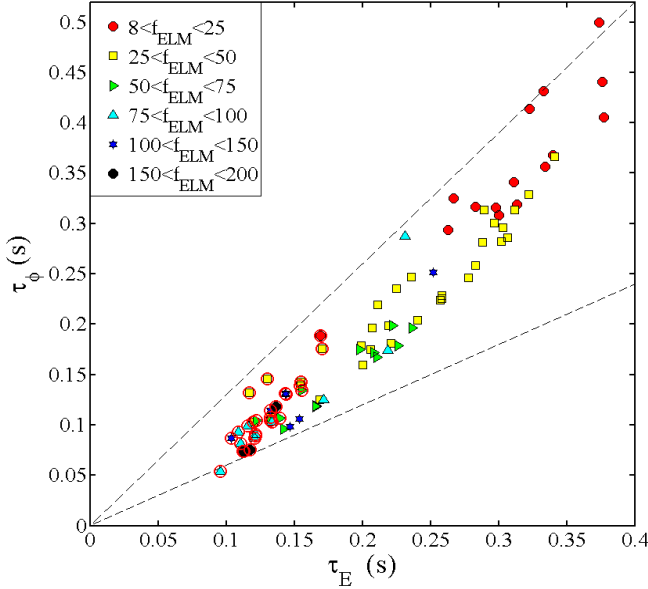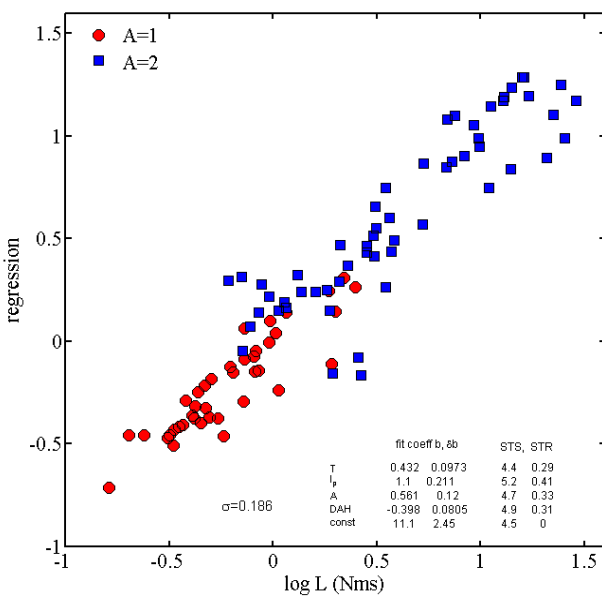

Fig.12 Angular momentum confinement time vs thermal energy confinement time. The symbols refer to ELM frequencies. Hydrogen plasmas are marked with an additional red circle. The broken lines corespond to $\tau_\phi/\tau_E=0.6$ and 1.3, respectively.

The total momentum L was obtained by volume integration of the local toroidal momentum density $l=\omega_\phi\rho_m R^2$, where ω_ϕ is the toroidal angular velocity from CXS, ρ_m the plasma mass density and R the distance from the torus axis. Fig.12 shows that the global momentum confinement time $\tau_\phi=L/T$, where T is the NBH torque calculated by PENCIL [Challis 1989], can range between 0.6 and 1.3 times the thermal energy confinement time, consistently with earlier observations which show $\chi_\phi{\sim}0.8\chi_i$ [Weisen 2012]. A close relationship between the isotope scaling of energy and momentum confinement has already been observed in ASDEX [Bessenrodt-Weberpals 1993]. The highest ratios τ_ϕ/τ_E are obtained at the lowest ELM frequencies. As ELM frequencies correlate with gas puff rates and densities, the highest ratios τ_ϕ/τ_E also correspond to the lowest gas puff rates and the highest densities.

Momentum confinement is very similar to the global energy confinement (see eq.9), as seen in fig.13, where the total momentum was regressed as

$$L \propto A^{0.56\pm0.12}T^{0.43\pm0.09}I_p^{1.1\pm0.21}\Gamma^{-0.4\pm0.08} \qquad \text{(eq.11)}$$

Fig.13 Regression for global angular momentum L in Nms in ELMy H-modes correponding to eq.11.

This is significant as momentum is not transported by electrons, showing that the electrons cannot be responsible for the majority of heat transport in these discharges. The dominance of ion transport in JET discharges has also been documented in a comprehensive study of the interspecies power balance in JET [Weisen 2020] and is consistent with the ITG regime being the dominant transport regime in most JET plasmas with dominant NBH.

The negative dependency on Γ of L_ϕ in eq.11 is stronger than that of W_{th} in eq.9. It is not clear whether this is a result of ELM losses, which may have an electromagnetic component not shared with the thermal plasma, or a result of charge exchange losses.

5.3 Particle confinement in type I ELMy H-modes

The particle content can be regressed as

$$N_e \propto A^{0.57\pm0.05}\Gamma^{-0.24\pm0.03}f_{ELM}^{-0.12\pm0.03} \qquad \text{(eq.12)},$$
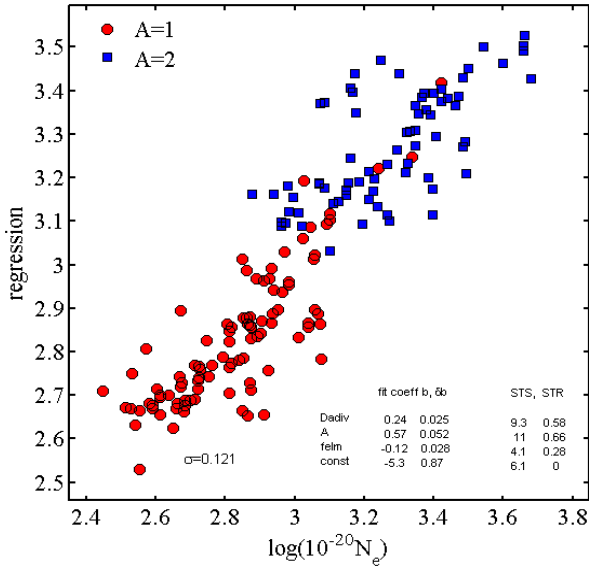
where f_{ELM} is the ELM frequency and Γ the Balmer-α emission from the divertor, measured using arrays vertically viewing both the inner and the outer divertor (fig.14).

Fig. 14. Regression for the total electron content according to eq.12. Dadiv stands for divertor Balmer-α emission and felm for the ELM frequency.

Unlike for energy and momentum confinement, it is the divertor emission and not the midplane emission that provides the best regression. The isotope mass is the most important contributor to this scaling (STR=0.66), well ahead of the ELM frequency (STR=0.28), showing that the differences in ELM frequency are not the only cause (and most likely not the main cause) for the lower density in hydrogen type I ELMy H-modes at low triangularity, as in these experiments. Remarkably, neither the heating power, nor the plasma current appear to have an impact on particle confinement, despite the proximity of a fraction of the cases to the Greenwald density limit [Greenwald 1988]. There is also no significant correlation between I_p and Γ.

The isotope dependence of particle confinement is similar to that for energy and momentum and suggest that the poor energy and momentum confinement in hydrogen H-modes may be due to the low particle confinement, in particular in the pedestal. Lower pedestal densities in hydrogen, combined with similar, stiff temperature profiles would lead to lower energy confinement. However, such a narrative wouldn't fit JT-60U results, from which no such difference in particle confinement is reported [Urano 2013], but instead, a difference in temperatures. At present the difference with JT-60U is not understood, and we limit our comparison to pointing out a few of the differences between the two devices, including the the usage of carbon PFC's in JT60-U, a substantially larger TF ripple in JT60-U leading to fast ion losses, which induce a torque directed counter to I_p, the usage of near perpendicularly injected low torque NBH for hydrogen, reinforcing fast ion losses. The JT-60U hydrogen plasmas were slowly counter-rotating ($\omega_\phi \sim -10^4$rad/s), while the deuterium plasmas were slowly co-rotating ($\omega_\phi \sim +10^4$rad/s)[Urano 2013]. JET ELMy H-modes plasmas with comparable NBH power co-rotated at much higher frequencies, ω_ϕ ranging from 3 to 7 $\times 10^4$rad/s.

Here, our liberal use of the Balmer-α emission as a proxy for the particle source deserves a discussion. This method is based on the approximate proportionality of Balmer-α photon emission rates and hydrogen isotope ionisation rates [Johnson & Hinnov 1973]. We find that in the above regressions, this emission leads to narrower fits than the usage of the gas injection rate into the vessel and therefore

accept them as better proxies for the particle flux into the plasma. It is however not clear why, for some cases, the main chamber Balmer-α emission provides narrower regressions than the divertor radiation or vice-versa. Strictly speaking, the edge source should only be inferred from Balmer-α emission from inside the last closed flux surface (LCFS). In practice this is close to impossible, except if tomographically inverted Balmer-α emission data from a tangentially viewing visible camera equipped with an interference filter are available, which was not the case for this study. Hence the light collected along single vertical or horizontal viewing lines will contain both emission from inside and outside the LCFS. The uncertainties concerning the spatial origin of this light are further acerbated by reflections at the metallic vessel walls. Divertor emission in the dataset is two orders of magnitude larger than main chamber emission, hence most of the light collected by divertor views originates from outside the LCFS. We therefore interpret divertor Balmer-α light as a likely proxy for the neutral density outside the LCFS, which is also proportional to the particle flux into the plasma.

5.4 Transport in mixed isotope ELMy H-modes

Experiments at I_p=1.4MA and B_T=1.7T with 8-10MW of NBH in mixed hydrogen/deuterium plasmas have allowed to scan the effective mass $A_{eff}=\Sigma_i A_i n_i / \Sigma_i n_i$ (for i=1,2) from 1 to 2 [King 2017, King 2020]. The isotope composition was inferred from the line intensity ratios of the Balmer-α lines of the two species, as measured from high resolution divertor spectroscopy [V.S. Neverov *et al* 2017]. Below 10MW, in pure hydrogen, a type I ELMy regime was not always achieved . Instead, these plasmas had type III ELMs and W_{th} ~0.8 MW. The pure hydrogen point, as well as the deuterium one, were taken from equivalent plasmas in the dataset presented in sections 5.2-5.4. The thermal stored energy in these discharges doesn't rise linearly with A_{eff}, instead exhibiting a plateau with near constant stored energy for $1.2 \leq A_{eff} \leq 1.8$, seen in fig.15 for $8 \leq P_{NBH} \leq 10$MW [D.B. King et al 2020]. While the plateau stored energy is constant, however, the pedestal density rises from near 2.3×10^{19}m^{-3} for A_{eff}<1.5 to about 3×10^{19}m^{-3} for A_{eff}=1.85, while at the same time the pedestal temperature drops from about 0.6keV to 0.5keV [King 2020]. The beam species for the mixed plasmas were also mixed, but consisted mostly of hydrogen and where therefore not matched to the bulk plasma composition established by adjusting the gas puff rates for the two species. This mismatch had no incidence of the confinement time, as shown by a comparison of pure hydrogen and pure deuterium injection at the same power into otherwise identical discharges.
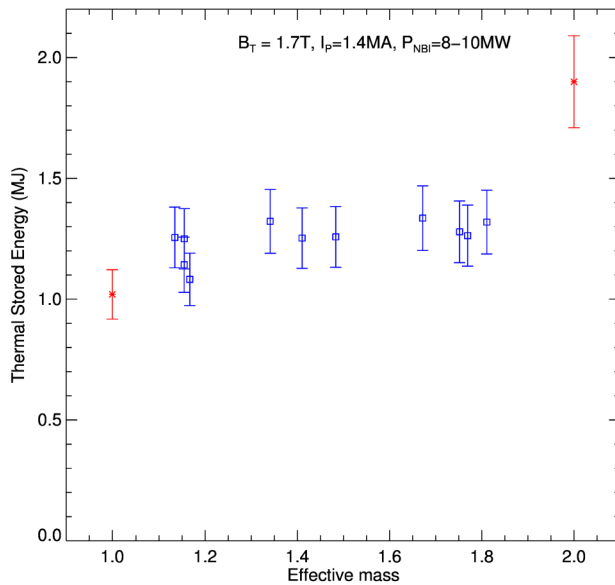

Fig.15 Thermal stored energy in isotope ratio scan at fixed current and power for H-mode plasmas with type I ELMS. The data points in red are from pure hydrogen and deuterium experiments. From [D.B. King et al 2020]

The plateau is reminiscent of a very similar plateau in L-H threshold power P_{L-H} observed in a different experiment [Hillesheim 2018]. This similarity may be linked to general observation that the confinement enhancement factor over IPB98 scaling [ITER Physics Basis, chapter 2, *Nucl. Fusion* **39,** 2175 (1999)] H-modes improves with P/P_{L-H}. These experiments were not repeated to establish the P_{L-H} threshold power, but from similar experiments [Hillesheim 2017] we estimate that in pure hydrogen plasmas P_{L-H} was barely exceeded, while for pure D it was higher than 2.

In several of the H-mode experiments deuterium NBH was used with a hydrogen background plasma. The core isotope composition was inferred from the measured neutron rates, showing that it only modestly exceeded the one measured using divertor Balmer-α spectroscopy [Maslov 2018]. As a result the shape of both ion isotope profiles remained close to that of the electrons. Transport simulations and quasilinear gyrokinetic modelling of the isotope profiles in these experiments have shown that the ion particle diffusion coefficient D_i can be as high as $2\chi_{\text{eff}}$ in the ITG mode, which, combined with strong inward convection leads to fast isotope mixing throughout the plasma cross section [Maslov 2018, Bourdelle 2018, Marin 2020]. This is in stark contrast with the electron particle transport, which governs the electron density profile and is characterised by transport coefficients an order of magnitude smaller than those for the ions. In TEM mode (not the case in these experiments), the ion transport coefficients from gyrokinetic modelling would be much smaller and isotope mixing is expected to be considerably slower [Bourdelle 2018] as observed in LHD [K. Ida 2020]. Core isotope ratio control has also been demonstrated by shallow (low penetration) deuterium pellets injected into a plasma simultaneously fuelled by hydrogen gas and hydrogen NBH [M. Valovic 2019]. A core H/D ratio $n_H/n_D \approx 1.2$, close to the target of $n_H/n_D = 1$, was obtained despite the different fuelling methods for the two species, as inferred from core hydrogen isotope CXS and from the neutron rates. Fast mixing greatly eases isotope ratio control, as it matters little (in ITG mode) how and where the main ion species are introduced into the plasma, boding well for isotope ratio control in the upcoming JET D-T experiments and in ITER.

5.5 Particle transport in the H-mode pedestal

Since core temperature profiles are essentially stiff (large variations in the heat flux only lead to small small variations of $R/L_T = R \nabla T/T$), pedestal conditions are the main contributor to the isotope effect manifested throughout the plasma in these JET-ILW experiments. The pedestal structure, MHD stability and ELM behaviour in hydrogen and deuterium ELMy H-modes have been extensively documented [L. Horvath 2020]. We here only summarise finding of direct relevance to the observed reduced particle confinement in hydrogen plasmas. At low ELM frequencies ($f_{ELM} < 40$ Hz) ELM particle losses increase with ELM frequency, correlating with lower pedestal top densities and showing that the increased ELM frequencies may contribute to lower hydrogen edge densities. Pedestal top densities in both species are similar at similar ELM frequencies. However there isn't a unique relationship between the particle loss rate attributable to the ELMs ($f_{ELM} \Delta N_{ELM}$, where ΔN_{ELM} is the number of particles lost per ELM) and the pedestal density, suggesting that other mechanisms, such as particle transport other than by ELMs also play a role [L. Horvath 2020 PhD thesis, L. Horvath 2020 sub. NF]. This observation is consistent with the regression (eq.12), which identifies the ELMs as a significant, but not the main, player in determining the plasma particle content.

The necessity for stronger fuelling in hydrogen is at odds with popular conceptions of fuelling by neutral penetration, as for all other parameters being equal (e.g. T_i), hydrogen neutrals should penetrate deeper into the plasma, thanks to their greater thermal velocity. The observation suggests that transport processes in the pedestal may overcome the effect of thermal velocity. The pedestal width model [Groebner] based on neutral penetration is inconsistent with observations of hydrogen and deuterium pedestals. This model predicts a pedestal width scaling as

$\Delta_{ne} \propto v_n r_i^{-1} n_{eped}^{-1} \propto A^{-1/2} n_{eped}^{-1}$, where v_n is the neutral velocity and r_i the ionisation rate, which is temperature dependent. At 1.4MA/1.7T there is no clear dependence of Δ_{ne} on species, nor on n_{eped}. In the 1MA/1T subset the measured widths, taken shortly before the ELM crashes, deviate by a factor two from the scaling (see e.g. fig.11 in [Weisen 2018]). This remains the case even when the effects of the temperature dependent neutral velocity and ionisation rates are taken into account [Horvath 2019 PhD thesis, 2020 NF subm.]. This shows that the pedestal density width cannot be inferred from neutral penetration alone. We conclude that transport processes, still poorly understood, also contribute to
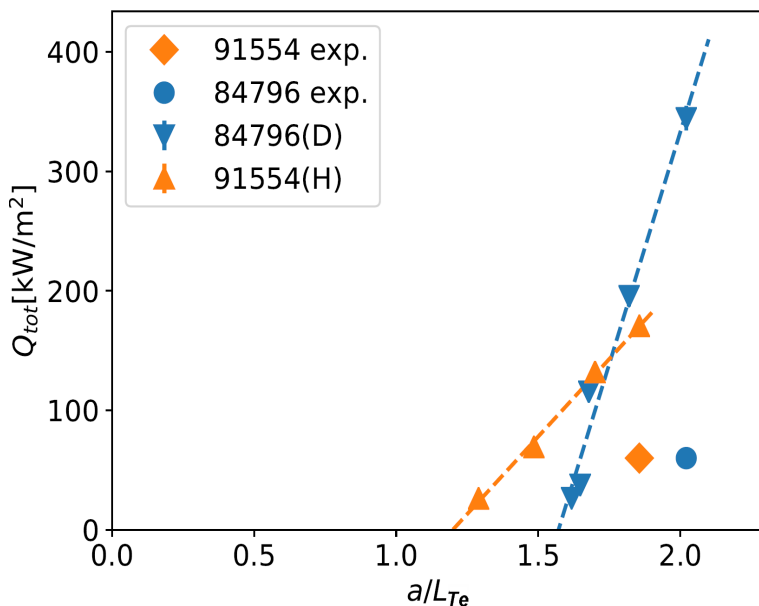
shaping the pedestal.

EDGE2D EIRENE [Somonini 1994, Wiesen 2006] was used to model the plasma boundary and pedestal region of a pair of H-modes in the two species. Both species required a transport barrier to model the pedestal and near SOL of 3cm width. In hydrogen the required particle diffusion coefficient was as much as 5 times higher than in deuterium. When only the isotope was changed to hydrogen in a simulation for deuterium, there was only a modest change in T_e and n_e profiles, which was opposite in sign to the observations. The analysis shows that plasma density profiles in the boundary are governed also by particle transport processes and are more complex than expected from neutral fuelling physics only. We expect better insights into the nature of transport in the H-mode pedestal and its dependence on the isotope species from gyrokinetic modelling (like the one in ref [Bonanomi 2019] for the L-mode edge) in conjunction with the application of MHD stability constraints.

5.6 Non-linear gyrokinetic modelling of core heat transport in hydrogen and deuterium type I ELMy H-modes

A pair of hydrogen and deuterium discharges with same heating power (10MW) from the type I ELMy H-mode dataset, has been analysed with flux-tube simulations at $\rho=0.5$ using the gyrokinetic code GENE [F. Jenko 2000, T. Görler 2011] and assuming $T_i=T_e$. The hydrogen plasma had a lower volume average density, electron temperature and thermal stored energy ($<n_e>=2.1\times10^{19}m^{-3}$, $T_e(0)=2.9keV$, $W_{th}=1.25MJ$) than the deuterium plasma ($<n_e>=2.8\times10^{19}m^{-3}$, $T_e(0)=3.9keV$, $W_{th}=2.34MJ$). Linear simulations including the effect of collisions show no significant deviations from Gyro-Bohm scaling. Nonlinear electromagnetic simulations including the effect of collisions using the standard drift-kinetic Landau-Boltzmann collision operator, E×B shear from the sheared rotation measured by CXS and dilution by Be impurities using the experimental temperature gradients lead to an over-prediction of the measured heat fluxes by a factor 2 for hydrogen and a factor 6 for deuterium, as seen in fig.16.

Fig.16 shows the result of a scan of normalised temperature gradient $a/L_{Te}=a\nabla T_e/T_e$ at $\rho_t=0.5$, where a is the minor radius, performed in order to find a match for the experimental heat flux. They show that the simulated heat fluxes can be approximately matched by reducing the temperature gradients by 20% in the hydrogen discharge and by 17% in deuterium. The simulations also show that deuterium transport is stiffer than the hydrogen one, but has the advantage of a higher instability threshold. At the modest heat flux in the experiment, $Q_{tot}\approx70kW/m^3$, below the crossing point where Q_{tot} is the same for both isotopes, this allows for steeper gradients and hence larger temperatures in the deuterium case.

Fig.16 Scan of mid-radius heat flux versus normalised gradient $a/L_{Te}=-a\nabla T_e/T_e$ calculated by GENE versus temperature gradient, assuming $T_i=T_e$. Orange : hydrogen, Blue : deuterium. The experimental points are shown as a diamond (hydrogen) and a dot (deuterium).
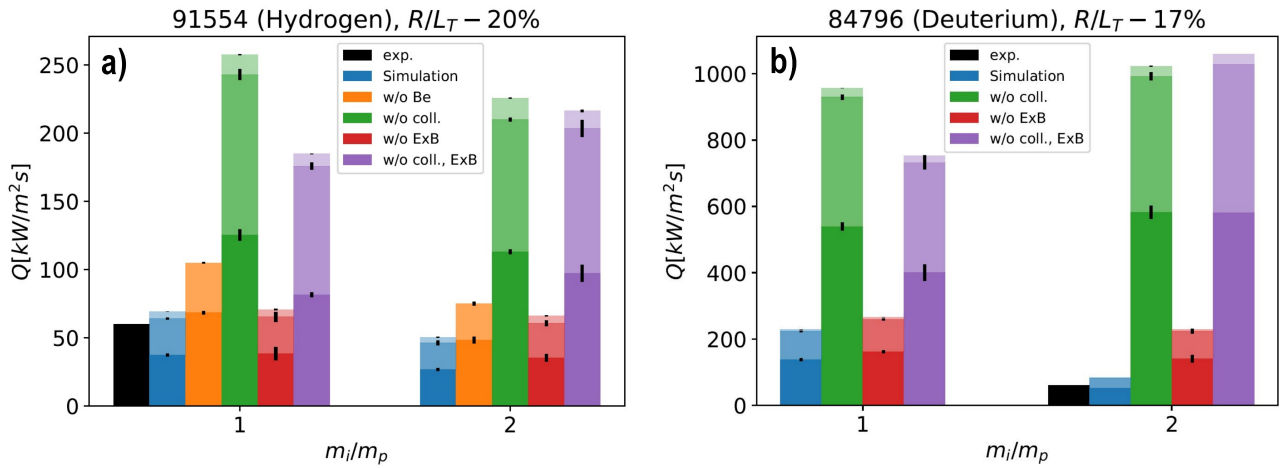
Fig. 17 Summary of non-linear GENE simulations in hydrogen and deuterium ELMy H-modes. Both discharges were simulated assuming A=1 and A=2.
Black bars : experimental heat flux (same in a) and b)), blue bars : complete simulation with all effects. Other bars : simulations with one or more effects left out. The bars in violet are for a case when both collisions and E×B shear from bulk toroidal rotation are excluded.
The divisions of the bars into parts with different shading indicate, from bottom to top, the ion, electron and Be contributions to the total heat flux.

Fig. 17 shows the results from a range of non-linear flux-tube GENE calculations at mid-radius undertaken to clarify the importance of collisions, E×B shear and dilution by Be impurities. For these calculations the gradients were adjusted, as indicated above, such as to obtain heat fluxes matching those of the experiment (black bars in fig. 17). For each discharge, simulations were performed assuming A=1 and A=2. In the absence of collisions, the simulated heat fluxes exceed the experimental ones by factors of 4-15 (green bars in fig 17). Collisions are essential for obtaining realistic heat fluxes, as seen when comparing the simulations without collisions (green bars) with those where E×B from sheared toroidal rotation (red) or impurities (orange) were left out. Collisions are seen to enhance the zonal flow shearing rate $\omega_{E\times B}$ spectra, reducing ITG amplitudes and suppressing TEM modes. Leaving out E×B from sheared toroidal rotation has little effect, except for the simulation of the D discharge wit A=2 (fig.17b). However the reduction by E×B stabilisation is always larger when A=2 is chosen in the simulations, than when A=1 is chosen, consistently with the qualitative sketch in fig.1. Neglecting Be impurities also leads to ~30% higher heat fluxes (fig.16 a), mainly as as a result of dilution of the mains species.

The effect of collisions is to cause a narrowing of the spectra of heat and particle fluxes by a factor 2 for hydrogen and a factor 3-4 for deuterium, as seen in fig.18. The figure shows the spectral heat and particle fluxes for 4 simulations based on the hydrogen experimental case, with (fig.18 a and b) and without (fig.18 c and d) collisions assuming A=1 (fig.18 a and c) and A=2 (fig.18 b and d). $k_y\rho_{sH}$ is the poloidal wavenumber normalised with the ion Larmor radius calculated for hydrogen. The figure shows both the electrostatic heat and particle fluxes (noted Q_{es} and Γ_{es}) and the magnetic flutter components (Q_{em} and Γ_{em}), which are comparatively small. In the absence of collisions, the peak amplitudes of the fluxes are higher for deuterium, although the spectral widths are somewhat smaller. The flux spectra are strongly affected by the collisions, becoming narrower and shifted to higher poloidal wavenumbers : $\langle k_y\rho_{sH}\rangle$~0.42 and ~0.36 with collisions for A=1 and 2 respectively and $\langle k_y\rho_{sH}\rangle$~0.3 and ~0.22 without collisions. Spectral amplitudes are only slightly reduced in the presence of collisions, hence the narrower spectra in deuterium are the main cause for the smaller fluxes. This spectral narrowing is due to electron-ion collisions suppressing TEM modes virtually completely. The stark differences between the cases in fig.18 are well apparent in the the cross phase

angle α between potential fluctuations and density fluctuations seen in fig. 19. The figure shows the probability distribution functions (PDFs) for the cross phase angle α as function of α and $k_y\rho_{sH}$, weighted as described in ref [T. Dannert 2005]. Outward particle transport occurs essentially for the positive angles in the region $k_y\rho_{sH}<0.6$. The region $k_y\rho_{sH}>0.6$ in fig.19 c) and d) (no collisions, no E×B shear) with finite PDF around $\alpha=\pm\pi$ is due to TEMs and is absent in the collisional cases with E×B shear (subplots a and b).

The resulting rms average of the zonal flow E×B shear rate is only about 10% larger in deuterium than in hydrogen in the fully collisional case, but about 1.55 times larger in deuterium when normalised to the respective thermal velocities. This suggests that the main contributor to the larger zonal flow E×B shear stabilisation in deuterium is the isotope effect discussed in the introduction (eq.1 and fig.1). The results are little changed when ion-ion collisions are left out of the calculations. With only electron-ion collisions, fluxes are reduced to a level within 15% of the full collisional case. This indicates that the reduced fluxes are primarily due to TEM suppression by electron-ion collisions.

These local non-linear GENE simulations at mid-radius show that a reversal of gyroBohm scaling is consistent with the experimental observations. This is highly encouraging, but we should keep in mind that we cannot extrapolate to global scaling from any local core transport model alone. It is very likely that in global nonlinear simulations with experimentally imposed boundary conditions, e.g. at the top of the pedestal, the global confinement will be strongly dependent on the boundary conditions as a result of profile stiffness, i.e. the root cause for the lower transport in deuterium in these plasmas is still to be sought in the pedestal. A different pedestal boundary condition (higher or lower pedestal temperature for the same heat flux) would lead to different core conditions (higher or lower core temperature for the same heat flux).
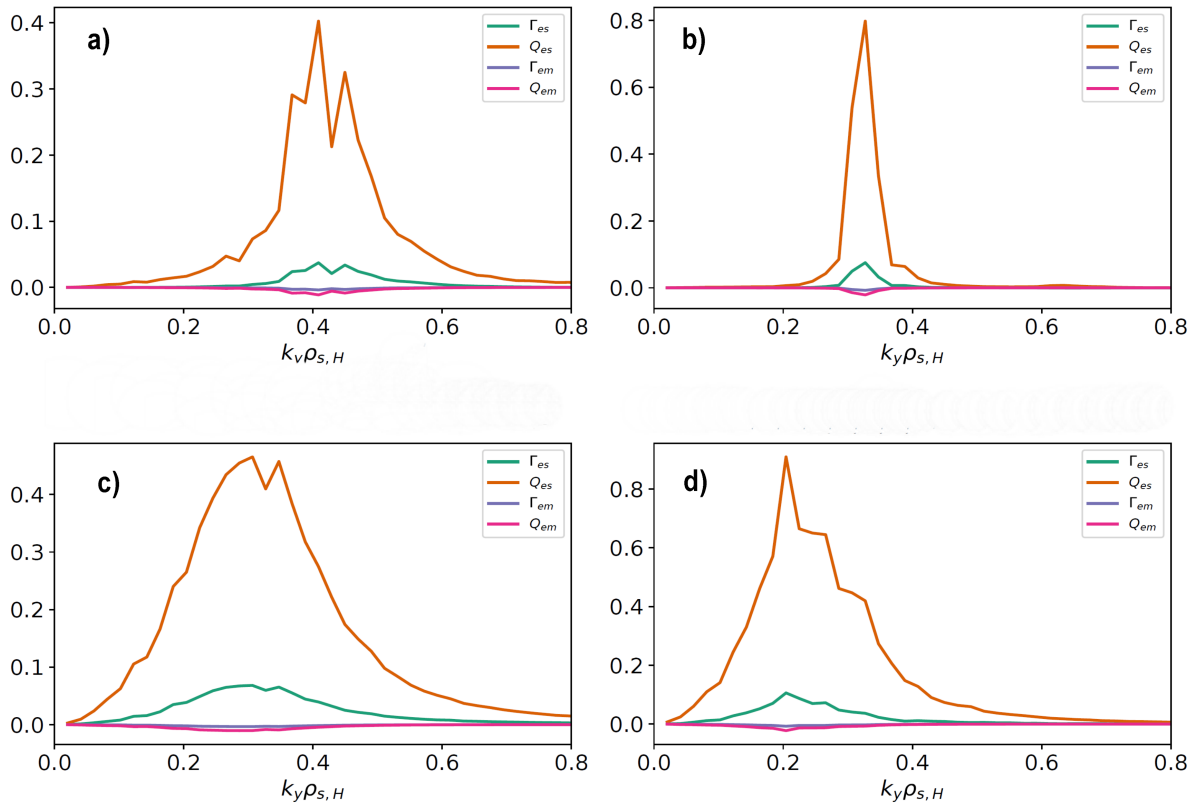

Fig. 18 Spectral heat and particle fluxes with collisions and rotational E×B shear (a and b) and without collisions nor E×B shear(c and d), assuming A=1 (a and c) and A=2 (b and d).
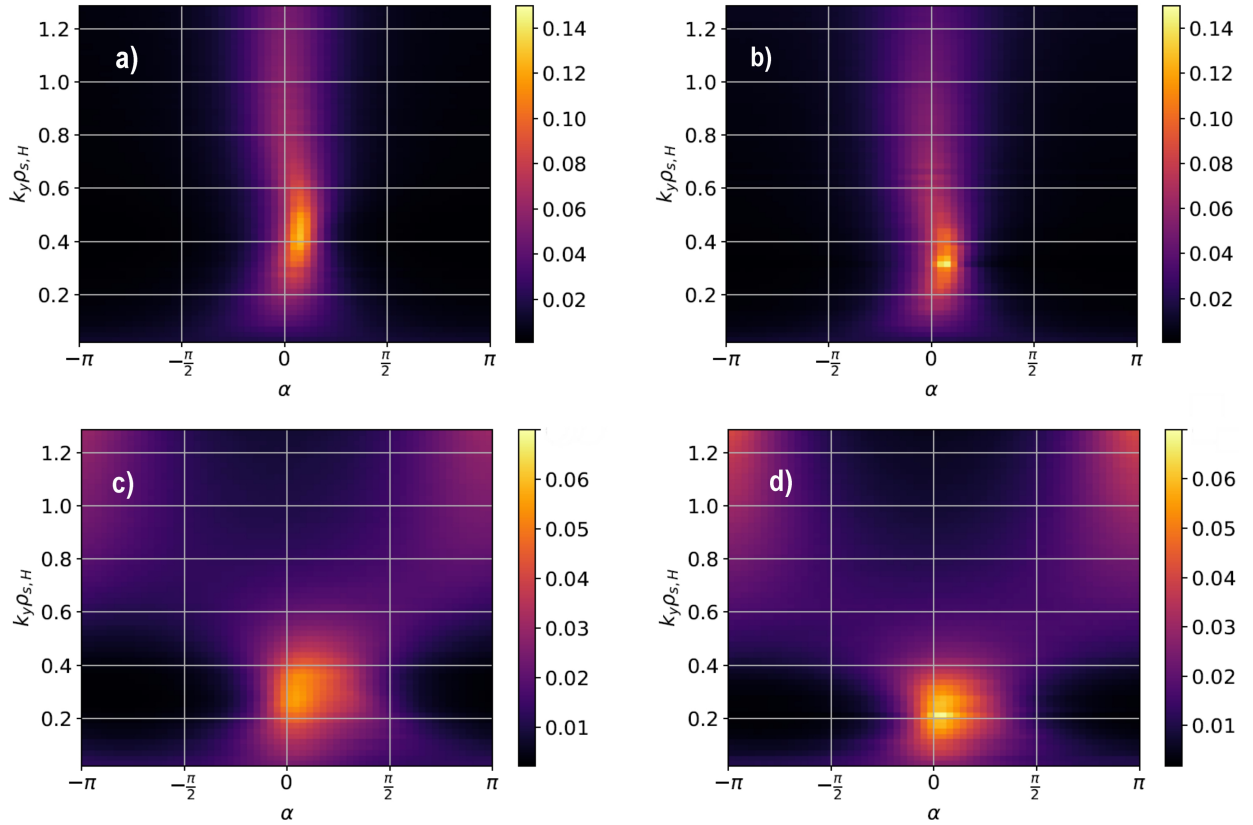
Fig. 19. Probability distributions for the cross angle between potential and density fluctuations for simulations with collisions and rotational E×B shear (a and b) and without collisions nor E×B shear(c and d), assuming A=1 (a and c) and A=2 (b and d).

6. Discussion

Following the JET results reported in [Maggi 2018], progress in data analysis and modelling has confirmed the scalings of the global energy confinement with isotope mass in L-mode (weak) and H-mode (strong) and extended them to include the momentum and the particle confinement. Remarkably, in H-mode all three transport channels, energy, momentum and particle transport, have similar isotope scalings, with mass exponents around 0.5. As a result of the observed and modelled temperature profile stiffness, the origin of global isotope scaling in the JET discharges investigated is sought for in the physics of the pedestal, which is sensitive to recycling, atomic physics processes and MHD stability. Analysis of density pedestal width shows that neutral fuelling physics alone is insufficient to explain the systematic differences between the species, pointing to the importance of transport processes in the pedestal that are species dependent and still need to be understood. Core confinement scales with pedestal conditions as a result of stiff temperature profiles in ITG dominated turbulence. This causes local gyroBohm scaling to be overidden in JETTO-TGLF simulations in L-mode, resulting in a prediction of independence of confinement on the isotope species. In non-linear flux-tube GENE simulations of the core of H-modes gyroBohm scaling is even reversed by the effect of collisions on zonal flow damping and to a lesser extent to the $\omega_{E\times B}$ shear and the effect of impurities.

The lessons from modelling work so far is that, within the realm of GK drift wave turbulence theory, there are several effects that can lead to a breaking gyroBohm scaling. The turbulence stabilising effects of E×B shear, whether from zonal flows or extrinsic (bulk rotation) are stronger for higher isotopic mass, which can lead to a suppression and even a reversal of gyroBohm scaling, depending on fluxes and boundary conditions. Electromagnetic effects at high beta can lead to a de-stiffening of ITG transport, which is stronger for higher ion mass [J. Garcia et al 2017] . Core transport must adopt a

transport state that is consistent with the boundary conditions (or the imposed local conditions in flux tube simulations) and the fluxes. If the boundary conditions are non-gyroBohm, then the core plasma establishes a corresponding non-gyroBohm transport state, as expected from the high degree of profile stiffness in ITG turbulence. This underlines the importance of understanding edge and pedestal transport and their isotope dependences. One may speculate that the isotope dependence of GK modelled transport in the edge plasma of L-modes also applies to H-modes [Bonanomi 2019], however specific simulations of H-mode pedestals will be required for progress. It would also be incorrect to assume that the core transport would always mirror the edge or pedestal transport. Core transport effects like rotational ExB shearing and fast ion electromagnetic stabilisation effects, which are stronger for plasmas with higher isotope mass, may compound the isotope effects at the edge or pedestal, leading to stronger core and global scaling with isotope mass than expected from boundary effects alone.

Unlike size and current scaling in the international databases [ITER Physics Basis, 1998 & 2007, Verdolaege 2018], which are robust ($\tau_E \sim I_p R^{1.6}$), there is no unique isotope scaling. The strength of the isotope dependence depends on operational parameters, on the confinement mode (L-mode, H-mode, TFTR 'supershot',...), the heating method, momentum injection and rotation, the wall materials and probably other yet to be identified parameters. In particular, edge and pedestal conditions are sensitive to recycling and atomic physics processes in ways which are still poorly understood, differ between devices and are difficult to diagnose and to control. We speculate that the above listed parameters, which vary widely between experiments, are at the origin of the wide range of isotope dependences reported in the literature. Ultimately, our traditional scaling expressions (we are disinclined to call them 'laws'), must be recognized as unable to capture multiple dependencies resulting from the wide variety of plasma conditions in fusion research devices and the intricate physics of plasma transport.

Acknowledgement

Referenceserparleiter6,
C.F. MAGGI, H. WEISEN, J.C. HILLESHEIM, A. CHANKIN, E. DELABIE, L. HORVATH, F. AURIEMMA, I. S. CARVALHO, G. CORRIGAN, J. FLANAGAN et al. 2018 *Plasma Phys. Control. Fusion* **60,** 014045
JET TEAM (prepared by M.L. WATKINS), *Physics of high performance JET plasmas in DT* 1999 Nucl. Fusion **39**, 1227-1244
G. SAIBENE, L.D. HORTON, R. SARTORI, B. BALET, S. CLEMENT, G.D. CONWAY, J.G. CORDEY, H.P.L. DE ESCH, L.C. INGESSON, J. LINGERTAT et al, 1999 *The influence of isotope mass, edge magnetic shear and input power on high density ELMy H modes in JET,* Nucl. Fusion **39** (1999) 1133
ITER PHYSICS EXPERT GROUPS ON CONFINEMENT AND
TRANSPORT AND CONFINEMENT MODELLING AND DATABASE, ITER PHYSICS BASIS EDITORS, in ITER Physics Basis 1999, *Chapter 2: Plasma confinement and transport*, Nucl. Fusion **39**, 2175
S.M. Kaye, M. Greenwald, U. Stroth, O. Kardaun, A. Kus, D. Schissel, J. DeBoo, G. Bracco, K. Thomsen, J.G. Cordey et al 1997 *ITER L mode confinement database,* Nucl. Fusion **37** 1303
M. BESSENRODT-WEBERPALS, F. WAGNER, ASDEX TEAM 1993 *THE ISOTOPE EFFECT IN ASDEX Nucl. Fusion* **33** 1205

J.G. CORDEY B. BALET, D.V. BARTLETT, R.V. BUDNYA, J.P. CHRISTIANSEN, G.D. CONWAY, L.-G. ERIKSSON, G.M. FISHPOOL, C.W. GOWERS, J.C.M. DE HAAS *et al* 1999 *Plasma confinement in JET H mode plasmas with H, D, DT and T isotopes* Nucl. Fusion **39** 301

C.F. MAGGI, L. FRASSINETTI, L. HORVATH, A. LUNNISS, S. SAARELMA, H. WILSON , J. FLANAGAN , M. LEYLAND, I. LUPELLI, S. PAMELA et al 2017 *Studies of the pedestal structure and inter-ELM pedestal evolution in JET with the ITER-like wal*l, Nucl. Fusion **57** 116012

H. WEISEN, C.F. MAGGI, S. MENMUIR, L HORVATH, T.W. BACHE, F.J. CASSON, M. OBERPARLEITER, S. SAARELMA, F. AURIEMMA, A. CHANKIN et al. 2018, *Isotope Dependence of Confinement in JET-ILW Deuterium and Hydrogen Plasmas,* IAEA-FEC2018, Islamabad, India, 22-27.10.2028, EX/P1-4 (2018)

C.F. MAGGI, H. WEISEN, F.J. CASSON, F. AURIEMMA , R. LORENZINI, H. NORDMAN, E. DELABIE, F. ERIKSSON , J. FLANAGAN, D. KEELING et al 2019 *Isotope identity experiments in JET-ILW with H and D L-mode plasmas*, Nucl. Fusion **59** 076028

S. D. SCOTT, M. C. ZARNSTORFF, CRIS W. BARNES, R. BELL, N. L. BRETZ, C. BUSH, Z. CHANG, D. ERNST, R. J. FONCK, L. JOHNSON et al 1995, *Isotopic scaling of confinement in deuterium–tritium plasmas*, Physics of Plasmas **2**, 2299 https://doi.org/10.1063/1.871253

D.R. ERNST B. COPPI, S. D. SCOTT, M. PORKOLAB, AND TFTR GROUP et al 1998, *Unifying Role of Radial Electric Field Shear in the Confinement Trends of TFTR Supershot Plasmas,* Phys. Rev. Lett. **81**, 2454

G.F. MATTHEWS . M, BEURSKENS, S. BREZINSEK, M. GROTH, E. JOFFRIN. A. LOVING, M. KEAR, M.-L. MAYORAL, R, NEU, P PRIOR et al 2011 *JET ITER-like wall—overview and experimental programme,* Phys. Scr. T145 014001

E.J. DOYLE, W.A. HOULBERG, Y. KAMADA, V. MUKHOVATOV, T.H. OSBORNE, A. POLEVOI, G. BATEMAN, J.W. CONNOR, J.G. CORDEY, T. FUJITA et al 2007, in ITER Physics Basis, Chapter 2: Plasma confinement and transport, Nucl. Fusion 47 S18-S127

G. VERDOOLAEGE, S.M. KAYE, C. ANGIONI, O.J.W.F. KARDAUN, F. RYTER, K. THOMSEN, THE ASDEX UPGRADE TEAM, THE EUROFUSION MST1 TEAM, M. MASLOV, M. ROMANELLI and JET CONTRIBUTORS 2018, *FIRST ANALYSIS OF THE UPDATED ITPA GLOBAL H-MODE CONFINEMENT DATABASE,* **27**th IAEA Fusion Energy Conference 22–27 October 2018 Ahmedabad, India https://nucleus.iaea.org/sites/fusionportal/Shared%20Documents/FEC%202018/fec2018-preprints/preprint0229.pdf

X. GARBET P. MANTICA, F. RYTER, G. CORDEY, F. IMBEAUX, C. SOZZI, A. MANINI, E. ASP, V. PARAIL, R. WOLF et al 2004, *Profile stiffness and global confinement*, Plasma Phys. Control. Fusion **46** 1351

J. CITRIN, F. JENKO, P. MANTICA, D. TOLD, C. BOURDELLE, R. DUMONT, J. GARCIA, J.W. HAVERKORT, G.M.D. HOGEWEIJ, T. JOHNSON, M.J. PUESCHEL et al 2014, *Ion temperature profile stiffness: non-linear gyrokinetic simulations and comparison with experiment,* Nucl. Fusion **54** 023008

H. BIGLARI , P. H. DIAMOND AND P.W. TERRY 1990, *Influence of sheared poloidal rotation on edge turbulence,* Phys. Fluids **B 2**, 1

M.N. ROSENBLUTH AND F.L. HINTON 1998 *Poloidal Flow Driven by Ion-Temperature-Gradient Turbulence in Tokamaks,* Phys. Rev. Lett. **80** 724

T. S. HAHM AND K.H. BURRELL 1995, *Flow shear induced fluctuation suppression in finite aspect ratio shaped tokamak plasma,* Phys. Plasmas **2**, 1648

T S Hahm and K H Burrell 1996, *Role of flow shear in enhanced core confinement regimes,* Plasma Phys. Control. Fusion **38** 1427–1431

R.E. WALTZ, R. L. DEWAR AND X. GARBET 1988, *Theory and simulation of rotational shear stabilization of turbulence*, Physics of Plasmas **5**, 1784 (1998); https://doi.org/10.1063/1.87284

J. CITRIN, J. GARCIA, T. GÖRLER, F. JENKO, P. MANTICA, D. TOLD, C. BOURDELLE,

D. R. HATCH, G. M. D. HOGEWEIJ et al 2015, *Electromagnetic stabilization of tokamak microturbulence in a high-β regime,* Plasma Phys. Control. Fusion **57** 014032

J. GARCIA, C. CHALLIS, J. CITRIN, H. DOERK, G. GIRUZZI, T. GÖRLER, F. JENKO, P. MAGET et al 2015, *Key impact of finite-beta and fast ions in core and edge tokamak regions for the transition to advanced scenarios*, Nucl. Fusion **55** 053007

A. DI SIENA T. GÖRLER , H. DOERK, R. BILATO, J. CITRIN , T. JOHNSON , M. SCHNEIDER, E. POLI, *Non-Maxwellian fast particle effects in gyrokinetic GENE simulations* Phys. of Plasmas **25**, 042304 (2018)

H. URANO, T. TAKIZUKA, M. KIKUCHI, T. NAKANO, N. HAYASHI, N. OYAMA AND Y. KAMADA 2012, *Small Ion-Temperature-Gradient Scale Length and Reduced Heat Diffusivity at Large Hydrogen Isotope Mass in Conventional H-Mode Plasmas*, *Phys. Rev. Lett.* **109** 125001

H. URANO, T. TAKIZUKA, N. AIBA, M. KIKUCHI, T. NAKANO, T. FUJITA, N. OYAMA, Y. KAMADA, N. HAYASHI AND THE JT-60 TEAM, 2013, *Hydrogen isotope effects on ITG scale length, pedestal and confinement in JT-60 H-mode plasmas*, Nucl. Fusion **53** 083003

F.W. PERKINS, CRIS W. BARNES, D. W. JOHNSON, S. D. SCOTT, M. C. ZARNSTORFF, M. G. BELL, R. E. BELL, C.E. BUSH, B. GREK, K. W. HILL et al, 1993, *Nondimensional transport scaling in the Tokamak Fusion Test Reactor: Is tokamak transport Bohm or gyro-Bohm?* Physics of Fluids B: Plasma Physics **5,** 477 https://doi.org/10.1063/1.860534

J.D. HUBA 2013, NRL PLASMA FORMULARY http://library.psfc.mit.edu/catalog/online_pubs/NRL_FORMULARY_13.pdf

W. HORTON 1999, *Drift waves and transport,* Rev. Mod. Phys. **71**, 735

D. BOHM 1949, *The characteristics of electrical discharges in magnetic fields,* A. Guthrie and R. K. Wakerling (eds.), New York: McGraw-Hill.

L. SPITZER 1960, *Particle Diffusion across a Magnetic Field*, Physics of Fluids **3** 659 doi:10.1063/1.1706104

W. HORTON, DUK-IN CHOI, AND W. M. TANG, 1981, *Toroidal drift modes driven by ion pressure gradients,* Physics of Fluids **24**, 1077 (1981); doi: 10.1063/1.863486

R.E. WALTZ, *Numerical simulation of electromagnetic turbulence in tokamaks,* 1985, The Physics of Fluids 28, 577 doi: 10.1063/1.865123

C. BOURDELLE, J. CITRIN, B. BAIOCCHI, A. CASATI, P. COTTIER, X. GARBET, F. IMBEAUX, 2016, *Core turbulent transport in tokamak plasmas: bridging theory and experiment with QuaLiKiz* Plasma Phys. Control. Fusion **58,** 014036

C. C. PETTY, T. C. LUCE, R. I. PINSKER, K. H. BURRELL, S.C. CHIU, P. GOHIL, R. A. JAMES AND D. WROBLEWSKI 1995, *Gyroradius Scaling of Electron and Ion Transport,* Phys. Rev. Lett. **74** 1763

I. PUSZTAI, J. CANDY, AND P. GOHIL 2011, *Isotope mass and charge effects in tokamak plasmas***,** Phys. Plasmas **18**, 122501 https://doi.org/10.1063/1.3663844

P. H. DIAMOND, S.-I. ITOH, K. ITOH, T. S. HAHM, 2005, *Zonal flows in plasma—a review*, Plasma Phys. Control. Fusion **47**, R35-R161, 2005 https://doi.org/10.1088/0741-3335/47/5/R01

T.S. HAHM, LUWANG, W.X.WANG, E.S. YOON AND F.X. DUTHOIT, 2013 *Isotopic dependence of residual zonal flows*, Nucl. Fusion 53 072002

F. Jenko, W. Dorland, M. Kotschenreuther and B. N. Rogers, 2000, *Electron temperature gradient driven turbulence,* Phys. Plasmas **7**, 1904

T. Görler, X. Lapillonne, S. Brunner, T. Dannert, F. Jenko, F. Merz and D. Told, 2011, *The global version of the gyrokinetic turbulence code GENE*, Journal of Computational Physics **230**, 7053

A. BUSTOS, A. BAÑÓN NAVARRO , T. GÖRLER, F. JENKO, AND C. HIDALGO, 2015, *Microturbulence study of the isotope effect,* Phys. Plasmas **22**, 012305 https://doi.org/10.1063/1.4905637

F. L. HINTON, *Thermal confinement bifurcation and the L- to H-mode transition in tokamaks*, Physics of Fluids B: Plasma Physics **3,** 696 (1991);

M. NAKATA, M. NUNAMI, H. SUGAMA, AND T.-H. WATANABE 2017, *Isotope Effects on Trapped-Electron-Mode Driven Turbulence and Zonal Flows in Helical and Tokamak Plasmas* Phys. Rev. Lett. **118**, 165002

C. ANGIONI, E. FABLE, P. MANAS, P. MANTICA, P. A. SCHNEIDER, ASDEX UPGRADE TEAM, EUROFUSION MST1 TEAM, AND JET CONTRIBUTORS, 2018, *Dependence of the turbulent particle flux on hydrogen isotopes induced by collisionality,* Phys. Plasmas **25**, 082517
https://doi.org/10.1063/1.5045545
E.A. BELLI J. CANDY AND R. E. WALTZ, 2019, *Reversal of turbulent gyroBohm isotope scaling due to nonadiabatic electron drive*, Phys. Plasmas **26**, 082305
https://doi.org/10.1063/1.5110401
N. BONANOMI C. ANGIONI, P.C. CRANDALL, A. DI SIENA , C.F. MAGGI,
P.A. SCHNEIDER, THE ASDEX UPGRADE TEAM, THE EUROFUSION MST1 TEAM
AND JET CONTRIBUTORS, 2019, *Effect of the isotope mass on the turbulent transport at the edge of L-mode plasmas in ASDEX Upgrade and JET-ILW* Nucl. Fusion **59** 126025
N. BONANOMI, I. CASIRAGHI P. MANTICA, C. CHALLIS, E. DELABIE, E. FABLE, D. GALLAR , C. GIROUD, E. LERCHE, P. LOMAS et al, 2019, *Role of fast ion pressure in the isotope effect in JET L-mode plasmas,* 2019 Nucl. Fusion **59** 096030
J. GARCIA, T. GÖRLER, F. JENKO AND G. GIRUZZI 2017 *Gyrokinetic nonlinear isotope effects in tokamakplasmas* Nucl. Fusion **57** 014007
J. GARCIA, T. GÖRLER AND F. JENKO 2018, *Isotope and fast ions turbulence suppression effects: Consequences for high-β ITER plasmas,* Phys. Plasmas **25**, 055902 (2018);
https://doi.org/10.1063/1.5016331
G. BATEMAN*, A.* H. KRITZ*,* V.V. PARAIL*,* J. G. CORDEY AND THE JET TEAM, 1999, *Effect of isotope mass on transport simulations of Joint European Torus high-mode plasmas with Edge Localized Modes* Physics of Plasmas **6**, 4607 doi: 10.1063/1.873724
P.A. SCHNEIDER, A. BUSTOS, P. HENNEQUIN, F. RYTER, M. BERNERT, M. CAVEDON, M.G. DUNNE, R. FISCHER1, T. GÖRLER, T. HAPPEL et al, 2017, *Explaining the isotope effect on heat transport in L-mode with the collisional electron-ion energy exchange* Nucl. Fusion **57** 066003
E DELABIE, M.M.F. NAVE , M. BARUZZO , J. BERNARDO , J. BOOM , J. BUCHANAN , N. HAWKES , J.C. HILLESHEIM , C.F. MAGGI , S. MENMUIR , E.R. SOLANO et al, 2017, *Preliminary interpretation of the isotope effect on energy confinement in Ohmic discharges in JET-ILW* **44**th EPS Conference on Plasma Physics, Belfast, 26-30 June 2017
http://ocs.ciemat.es/EPS2017PAP/pdf/P4.159.pdf
F.M. LAGGNER, E. WOLFRUM, M. CAVEDON, F. MINK, M. BERNERT, M. G. DUNNE, P. A. SCHNEIDER, A. KAPPATOU, G. BIRKENMEIER, R. FISCHER et al, 2017, *Pedestal structure and inter-ELM evolution for different main ion species in ASDEX Upgrade,* Phys. Plasmas, **24** 056105
L. FRASINETTI, M. N. A. BEURSKENS, R. SCANNELL, T. H. OSBORNE, J. FLANAGAN, M. KEMPENAARS, M. MASLOV, R. PASQUALOTTO, M. WALSH, and JET-EFDA Contributors, *2012, Spatial resolution of the JET Thomson scattering system,* Review of Scientific Instruments **83**, 013506
M. MASLOV, M.N.A. BEURSKENS, M. KEMPENAARS AND J. FLANAGAN, 2013, *Status of the JET LIDAR Thomson scattering diagnostic* Journal of Instrumentation **8** C11009
 https://iopscience.iop.org/article/10.1088/1748-0221/8/11/C11009/pdf
C. Giroud, A. G. Meigs1*,* C. R. Negus1*,* K.-D. Zastrow1*,* T. M. Biewer2*,* T. W. Versloot3*,* and JET-EFDA Contributors 2008, *Impact of calibration technique on measurement accuracy for the JET core charge-exchange system,* Rev. Sci. Instrum. **79** 525 https://aip.scitation.org/doi/10.1063/1.2974806
A.E. SHUMACK, J. RZADKIEWICZ*,* M. CHERNYSHOVA*,* K. JAKUBOWSKA, M. SCHOLZ*,* A. BYSZUK*,* R. CIESZEWSKI*,* T. CZARSKI*,* W. DOMINIK*,* L. KARPINSKI et al, 2014, *X-ray crystal spectrometer upgrade for ITER-like wall experiments at JET,* Review of Scientific Instruments **85**, 11E425 (2014);

H. WEISEN, E. DELABIE, J. FLANAGAN, C. GIROUD, M. MASLOV, S. MENMUIR, A. PATEL, S. SCOTT, P. SIREN, J. VARJE 2020, *Analysis of the inter-species power balance in JET plasmas,* Nucl. Fusion **60** 036004 https://iopscience.iop.org/article/10.1088/1741-4326/ab6307/pdf

V.S. NEVEROV, A.B. KUKUSHKIN, M.F. STAMP, A.G. ALEKSEEV, S. BREZINSEK, M. VON HELLERMANN AND JET CONTRIBUTORS 2017 *Determination of divertor stray light in high resolution main chamber H α spectroscopy in JET-ILW,* Nucl. Fusion **57** 016031

U. KRUEZI G. SERGIENKO, P. D. MORGAN, G. F. MATTHEWS, S. BREZINSEK, S. VARTANIAN, AND JET-EFDA CONTRIBUTORS , 2012, *JET divertor diagnostic upgrade for neutral gas analysis,* Rev.Sci. Instrum. **83** (2012) 10D728

M. MASLOV, D.B. KING, E. VIEZZER , D.L. KEELING, C. GIROUD, T. TALA, A. SALMI, M. MARIN, J. CITRIN, C. BOURDELLE et al, 2018, *Observation of enhanced ion particle transport in mixed H/D isotope plasmas on JET*, Nucl. Fusion **58** 076022

D.B. KING, E. VIEZZER, I. BALBOA, M. BARUZZO, E. BELONOHY, J. BUCHANAN, I.S. CARVALHO, K. CAVE-AYLAND, I. COFFEY, C.D. CHALLIS et al 2020 *Mixed Hydrogen-Deuterium plasmas on JET ILW*, submitted to Nucl. Fusion

D.B. KING, E. VIEZZER , M. BARUZZO , E. BELONOHY , J. BUCHANAN , I CARVALHO , K. CAVE-AYLAND , I. COFFEY , C.D. CHALLIS , E.G. DELABIE et al, 2017, *Mixed Hydrogen-Deuterium plasmas on JET ILW: H-mode confinement and isotope mixture control* , **44**th EPS Conference on Plasma Physics, Belfast, http://ocs.ciemat.es/EPS2017PAP/pdf/O3.112.pdf

J. C. HILLESHEIM, E. DELABIE, E. R. SOLANO, I.S. CARVALHO, A. DRENIK, C. GIROUD , A. HUBER , E. LERCHE , B. LOMANOWSKI, M. MANTSINEN et al 2017, *L-H transition studies in hydrogen and mixed ion species plasmas in JET,* **44**th EPS Conf. On Plasma Physics (Belfast, June 2017) P5.162 http://ocs.ciemat.es/EPS2017PAP/pdf/P5.162.pdf

O. KARDAUN 2005, *Classical Methods of Statistics*, ISBN-10 3-540-21115-2, Springer

GENERAL ATOMICS, "*EFIT Equilibrium and Reconstruction Fitting Code*" https://omfit.io/modules/mod_EFIT.html

C.D. Challis, J.G. CORDEY, H. HAMNEN, P.M. STUBBERFIELD, J.P. CHRISTIANSEN, E. LAZZARO, D.G. MUIR, D. STORK, E. THOMPSON et al. 1989, *Non-inductively driven currents in JET* Nucl. Fusion **29** 563

W. A. COOPER AND A. J. WOOTTON 1982, β_p *analysis for Tokamak plasma with anisotropic pressure and mass flow,* Plasma Phys. **24** 1183

M. FITZGERALD M. J. HOLE AND Z. S. QU 2015 *MHD normal mode analysis with equilibrium pressure anisotropy* Plasma Phys. Control. Fusion **57** 025018

G. STAEBLER, , R. E. WALTZ and J. E. KINSEY   2007 *A theory-based transport model with comprehensive physics,* Phys. Plasmas **14** 055909

G. STAEBLER, N. HOWARD, J. CANDY AND C. HOLLAND, 2017, *A model of the saturation of coupled electron and ion scale gyrokinetic turbulence,* Nucl. Fusion **57** 066046, https://iopscience.iop.org/article/10.1088/1741-4326/aa6bee/meta.

C.F. MAGGI, S. SAARELMA, F.J. CASSON, C. CHALLIS, E. DE LA LUNA, L. FRASSINETTI, C. GIROUD1, E. JOFFRIN, J. SIMPSON, M. BEURSKENS et al, et al, 2015 *Pedestal confinement and stability in JET-ILW ELMy H-modes*, Nucl. Fusion **55** 113031

H. URANO, J. HOBIRK, C.F. MAGGI, E. JOFFRIN AND JET CONTRIBUTORS, 2016 *Characterization of electron density based on operational parameters in JET H-mode plasmas with C and ILW* **43**rd EPS Conf. on Plasma Physics (Louvain, June 2016) O4.121

M. MASLOV, A. BOBOC, M. BRIX, J. C. FLANAGAN, E. PELUSO, C. PRICE, M. ROMANELLI AND JET CONTRIBUTORS, 2020 *Energy and particle confinement in JET H-mode plasma* Nucl. Fusion **60** 036007

J. GARCIA, R.J. DUMONT, J. JOLY, J. MORALES, L. GARZOTTI, T.W. BACHE, Y. BARANOV, F.J. CASSON, C. CHALLIS, K. KIROV, J. MAILLOUX et al, 2019, *First principles and integrated modelling achievements towards trustful fusion power predictions for JET and ITER,* Nucl. Fusion **59**

086047

J.G. CORDEY, B. ALPER, R. BUDNY, J. P. CHRISTIANSEN, I. COFFEY, K. ERENTS, P. HARBOUR, L. D. HORTON, K. LAWSON, G F MATTHEWS, G SAIBENE *et al* 2000, *Isotope identity experiments in JET*, Plasma Phys. Control. Fusion **42** A127

J G CORDEY, B BALET, D CAMPBELL, C D CHALLIS, J P CHRISTIANSEN, C GORMEZANO, C GOWERS, D MUIR, E RIGHI, G R SAIBENE, P M STUBBERFIELD AND K THOMSEN 1996 *A review of the dimensionless parameter scaling studies ,* Plasma Phys. Control. Fusion **38** A67

C. BOURDELLE C. BOURDELLE, Y. CAMENEN, J. CITRIN, M. MARIN, F.J. CASSON, F. KOECHL, M. MASLOV AND THE JET CONTRIBUTORS, 2018, *Fast H isotope and impurity mixing in ion-temperature-gradient turbulence*, Nucl. Fusion **58** 076028

H. WEISEN, Y. CAMENEN, A. SALMI, T.W. VERSLOOT, P.C. DEVRIES, M. MASLOV, T. TALA, M. BEURSKENS, C. GIROUD AND JET-EFDA CONTRIBUTORS 2012, *Ubiquity of non-diffusive momentum transport in JET H-modes,* Nucl. Fusion 52 114024

M. GREENWALD, J.L. TERRY, S.M. WOLFE, S. EJIMA, M.G. BELL, S.M. KAYE AND G.H. NEILSON 1988, *A new look at density limits in tokamaks,* Nucl. Fusion **28** 2199.

L.C. JOHNSON AND E. HINNOV 1973, *Ionization, recombination, and population of excited states in hydrogen plasmas*, Quant. Spectrosc. Radiat. Transfer **13** (1973) 333

J.C. HILLESHEIM, E. DELABIE , E. R. SOLANO , C.F. MAGGI, H. MEYER, E. BELONOHY, I.S. CARVALHO, E. DE LA LUNA, A. DRENIK, M. GELFUSA, C. GIROUD et al, 2018, *Implications of JET-ILW L-H Transition Studies for ITER,* **27**th IAEA Fusion Energy Conference 22–27 October 2018 Ahmedabad, India https://nucleus.iaea.org/sites/fusionportal/Shared%20Documents/FEC%202018/fec2018-preprints/preprint0346.pdf

M. MARIN, J. CITRIN, C. BOURDELLE, Y. CAMENEN, F.J. CASSON, A. HO, F. KOECHL, M. MASLOV AND JET CONTRIBUTORS 2020, *First-principles-based multiple-isotope particle transport modelling at JET,* Nucl. Fusion **60** 046007

K. IDA, M. NAKATA, K. TANAKA, M. YOSHINUMA, Y. FUJIWARA, R. SAKAMOTO, G. MOTOJIMA, S. MASUZAKI, T. KOBAYASHI, AND K. YAMASAKI, 2020, *Transition between Isotope-Mixing and Nonmixing States in Hydrogen-Deuterium Mixture Plasmas,* Phys. Rev. Lett. **124**, 025002

M. VALOVIC, Y. BARANOV, A. BOBOC, J. BUCHANAN, J. CITRIN, E. DELABIE, L. FRASSINETTI, J.M. FONTDECABA, L. GARZOTTI, C. GIROUD, R. MCKEAN et al 2019 *Control of the hydrogen:deuterium isotope mixture using pellets in JET*, Nucl. Fusion **59** 106047

L. Horvath, (2019) *Isotope dependence of the H-mode pedestal in JET-ILW plasmas,* PhD thesis, University of York, UK, http://etheses.whiterose.ac.uk/id/eprint/27103

L. Horvath, C.F. Maggi, A. Chankin, S. Saarelma, A.R. Field, S. Aleiferis, E. Belonohy, A. Boboc, G. Corrigan, E.G. Delabie (2020) *Isotope dependence of the type I ELMy H-mode pedestal in JET-ILW Hydrogen and Deuterium plasmas,* submitted to Nuclear Fusion

R.J. GROEBNER, M. A. MAHDAVI, A. W. LEONARD, and T. H. OSBORNE 2002, *The role of neutrals in high-mode (H-mode) pedestal formation*, Phys. Plasmas **9** 2134 https://doi.org/10.1063/1.1462032

R. SIMONINI, G CORRIGAN,G RADFORD, J SPENCE AND A TARONI 1994, *Models and Numerics in the Multi-Fluid 2-D Edge Plasma Code EDGE2D/U*, Contributions to Plasma Physics, **34** (2-3):368-373

S. WIESEN. *EDGE2D/EIRENE code interface report*. IRC Report, June 30, 2006. http://www.eirene.de/e2deir_report_30jun06.pdf

T. DANNERT AND F. JENKO 2005, *Gyrokinetic simulation of collisionless trapped-electron mode turbulence*, Phys. Plasmas **12**, 072309 (2005); https://doi.org/10.1063/1.1947447